Electronic Supplementary Information for:

Metal-organic frameworks: new matrixes for surface-assisted laser desorption/ionization mass spectrometry*

Yung-Han Shih, Ching-Hsuan Chien, Brenda Singco, Chang-Lin Hsu, Chia-Her Lin* and Hsi-Ya Huang*

Department of Chemistry, Chung Yuan Christian University, 200 Chung Pei Road, Chung-Li, 320, Taiwan

*To whom correspondence should be addressed. E-mail: hyhuang@cycu.edu.tw, chiaher@cycu.edu.tw

Table of Contents

1. Preparation of MOFs
2. Preparation of analyte solutions
3. Sample preparation for MALDI- or SALDI-TOF MS.
4. Solid-phase extraction (SPE) prior to SALDI-TOF MS analysis with MOF as the adsorbent and matrix (scheme S1†)
5. Mass Spectrometry
6. Synthesis of 3.5-,14- and 33-nm Au NPs
7. Synthesis of SBA-15
8. UV-visible spectra of MOFs
9. MALDI-MS spectra of PAHs using CHCA as matrix
10. SALDI-MS spectra of PAHs using **MIL-100(Fe)** as matrix (Fig. S4)
11. SALDI-MS spectra of PAHs using **MIL-100(Cr)** as matrix (Fig. S5)
12. SALDI-MS spectra of PAHs using **MIL-100(Al)** as matrix (Fig. S6)
13. SALDI-MS spectra of PAHs using **MIL-101(Cr)** as matrix (Fig. S7)
14. SALDI-MS spectra of PAHs using **CYCU-3** as matrix (Fig. S8)
15. SALDI-MS spectra of PAHs using **DUT-4** as matrix (Fig. S9)
16. SALDI-MS spectra of PAHs using **DUT-5** as matrix (Fig. S10)
17. Laser induced ionization mass spectra of CYCU-3 and its synthetic precursor (Fig. S11)
18. SALDI-MS spectra of 4 PAHs using MIL-100(Fe) as matrix (Fig. S12)
19. SEM images of MOFs (Fig. S13)
20. ESCA spectra of MIL-100(Fe) (Fig. S14)
21. Micro FT-IR spectra of MIL-100 (Fig. S15)
22. Optical images of matrixes (Fig. S16)
23. SALDI-MS spectra of river water samples (Fig. S17)
24. SALDI-MS spectra of ester compounds (Fig. S18)
25. SALDI-MS spectra of anti-inflammatory drug (Fig. S19)
26. Powder X-ray diffraction (PXRD) patterns of MIL-100 (Fig. S20)
27. SALDI-MS spectra of PAHs using different nanoparticles as matrix (Fig. S21)
28. Mass spectra of laser desorption/ionization of PAHs without matrixes (Fig. S22)
29. The reproducibility of mass intensity for laser desorption/ionization analysis of benzo[ghi]perylene (Fig. S23)
30. Laser power effects on SALDI-MS analysis of benzo[a]pyrene using MOFs and NPs as matrixes. Each data was collected by 5 spectra. (Fig. S 24)
31. SALDI-MS analysis of benzo[a]pyrene via a) MIL-100(Fe); b) SBA-15; c) 3.5 nm Au; d) 14 nm Au; e) 33 nm Au as matrix with laser power of 58%.(Fig. S25)
32. SALDI-MS spectra of PAHs using 3.5 nm Au as matrix. (Fig. S26)

33. SALDI-MS spectra of PAHs using 33 nm Au as matrix. (Fig. S27)
34. Table S1 Reproducibility of signal intensity for BaP determined by SALDI-MS with CHCA and MIL-100(Fe) as matrix
35. Table S2 Literature survey for signal reproducibility using NPs as SALDI-MS matrix
36. Table S3 Porosity and surface area of the synthetic nanoparticles used in this work
37. Table S4 Characteristic of MOFs
38. Table S5 Reproducibility of PAHs signals with 3.5-,14-, 33- nm Au nanoparticles and MOFs as matrixes
39. Table S6 Comparison of MOFs and NPs in the preparation time, cost, background and reproducibility
40. Table S7 Effect of three sample preparation for BaP signal intensities using CHCA as matrix
41. Table S8 Various chromatographic methods for PAHs analysis
42. References

1. Preparation of MOFs

MIL-100(Fe), $[Fe_3F(H_2O)_2O(BTC)_2]\cdot 14.5H_2O$, was synthesized and activated with following method comparing published procedures (ref. S1).
Generally, **MIL-100(Fe)** was hydrothermally synthesized under microwave-assisted reactions. A mixture of iron nitrate nonahydrate ($Fe(NO_3)_3\cdot 9H_2O$, 404 mg, 1.0 mmol), trimesic acid ($C_9H_6O_6$, 141 mg, 0.67 mmol), HNO_3 (0.025 ml), HF (0.035 ml) and H_2O (5 ml) was placed in a 100 mL Teflon autoclave placed in a microwave oven. The mixture was heated at 180 °C for 30 min. The resulting light orange powderd sample was collected by filtration, washed with purified water and dried at room temperature. An activation conditions was applied by further heating 8 hr with water and EtOH. The **MIL-100(Fe)** was vacuumed and heated at 150 °C for 1 day before further experiments.

The chromium trimesate **MIL-100(Cr), [**$Cr_3F(H_2O)_2O(BTC)_2]\cdot 28.5H_2O$, was synthesized and activated according to published procedures (ref.S2).
Generally, **MIL-100(Cr)** was hydrothermally synthesized by a mixture of chromium nitrate nonahydrate ($Cr(NO_3)_3\cdot 9H_2O$: 400 mg, 1.0 mmol), trimesic acid ($C_9H_6O_6$, 141 mg, 0.67 mmol), HF (0.07 ml) and H_2O (5 ml) was placed in a 23 mL Teflon autoclave. The mixture was heated at 220 °C for 4 days. The resulting dark-green powdered sample was collected by filtration, washed with purified water and dried at room temperature. An activation conditions was applied by further reflux 4 hr with DMF and 1 day in EtOH. The **MIL-100(Cr)** was vacuumed and heated at 150 °C for 1 day before further experiments.

The aluminum MOF **MIL-100(Al), [**$Al_3(OH)(H_2O)_2O(BTC)_2]\cdot 24H_2O$, was synthesized and activated with following method comparing to published procedures (ref.S3).
Generally, **MIL-100(Al)** was hydrothermally synthesized under microwave-assisted reactions. A mixture of aluminum nitrate nonahydrate ($Al(NO_3)_3\cdot 9H_2O$: 664 mg, 1.77 mmol), trimethyl-1,3,5-trimesate ($(CH_3O)_3C_6H_3$, 380 mg, 1.19 mmol), HNO_3 (0.3 ml) and H_2O (6 ml) was placed in a 100 mL Teflon autoclave placed in a microwave oven. The mixture was heated at 200 °C for 30 min. The resulting yellowish powdered sample was collected by filtration, washed with purified water and dried at room

temperature. An activation conditions was applied by further microwave-assisted heating with 4 hr with DMF and reflux 1 day in water. The **MIL-100(Al)** was vacuumed and heated at 150 °C for 1 day before further experiments.

MIL-100

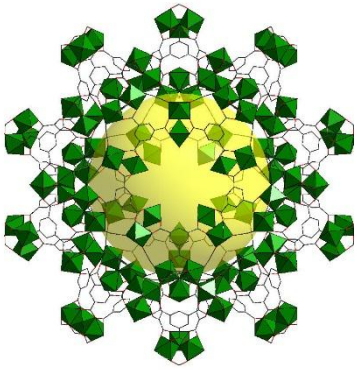

MIL-101(Cr), $[Cr_3O(BDC)_3(F)(H_2O)_2]\cdot 25H_2O$, was synthesized and activated according to published procedures (ref. S4).
Generally, **MIL-101(Cr)** was hydrothermally synthesized by a mixture of chromium nitrate nonahydrate ($Cr(NO_3)_3\cdot 9H_2O$: 400 mg, 1.0 mmol), terephthalic acid ($C_8H_6O_4$, 166 mg, 1.0 mmol), HF (0.2 ml) and H_2O (5 ml) was placed in a 23 mL Teflon autoclave. The mixture was heated at 220 °C for 8 hr. The resulting green powdered sample was collected by filtration, washed with purified water and EtOH and dried at room temperature. An activation conditions was applied by further heating 1 day in DMF then stir in EtOH for overnight. The **MIL-101(Cr)** was vacuumed and heated at 150 °C for 1 day before further experiments.

MIL-101

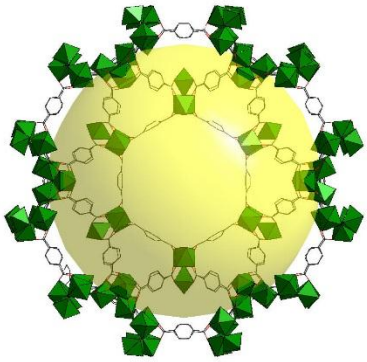

DUT-4, [Al(OH)(NDC)] and **DUT-5,** [Al(OH)(BPDC)] were synthesized according to published procedures (ref. S5).

Generally, **DUT-4** or **DUT-5** was hydrothermally synthesized under microwave-assisted reactions. A mixture of aluminum nitrate nonahydrate ($Al(NO_3)_3 \cdot 9H_2O$: 176 mg, 0.47 mmol), 2,6-naphthalenedicarboxylic acid ($C_{12}H_8O_4$, 86 mg, 0.4 mmol) or biphenyl-4,4'-dicarboxylic acid ($C_{14}H_{10}O_4$, 97 mg, 0.4 mmol), and dimethylformamide (DMF, 10.0 ml) was placed in a 100 mL Teflon autoclave placed in a microwave oven. The mixture was heated at 120 °C for 30 min. The resulting white powdered sample was collected by filtration, washed with DMF and dried at room temperature. The **DUT-4** or **DUT-5** was vacuumed and heated at 150 °C for 1 day before further experiments.

DUT-4

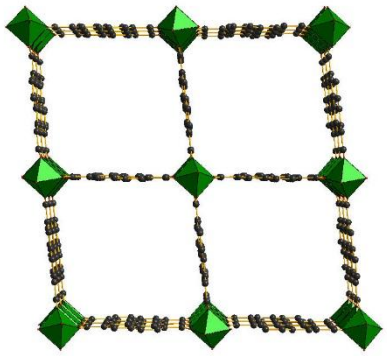

DUT-5

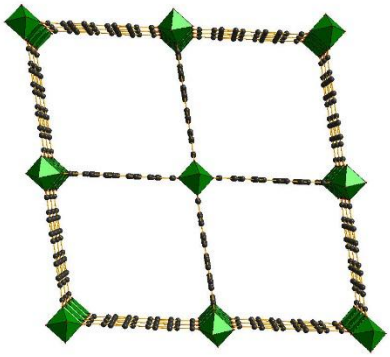

CYCU-3(Al), $[Al(OH)(SDC)] \cdot xH_2O$, was synthesized and activated according to published procedures (ref. S6).

Generally, a reaction mixture of 4,4'-stilbenedicarboxylic acid (H_2SDC, 107 mg, 0.40 mmol), aluminium chloride ($AlCl_3$, 54 mg, 0.4 mmol), and dimethylformamide (DMF, 10.0 ml) was heated at 180 °C for 3 days. A pale-yellow powder was filtered off, washed with DMF, dried at 90 °C. The **CYCU-3(Al)** was vacuumed and heated at 150 °C for 1 day before further experiments.

CYCU-3

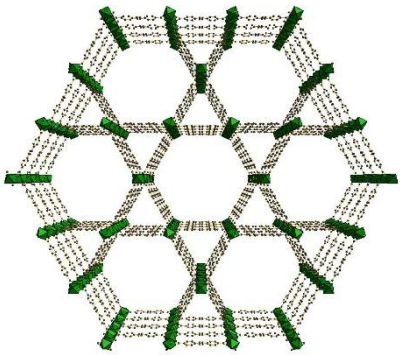

H_3BTC = 1,3,5-Benzenetricarboxylic acid

H_2BDC = 1,4-Benzenedicarboxylic acid

H_2NDC = 2,6-Naphthalenedicarboxylic acid

H_2BPDC = Biphenyl-4,4'-dicarboxylic acid

H_2SDC = 4,4'-stilbenedicarboxylic acid

2. Preparation of analyte solutions

Stock solutions of PAHs standards were dissolved in acetonitrile at a concentration of 500 μg/mL. Sample solutions at other concentrations were obtained by step dilution. All stock solutions were kept at ~4 °C for further use.

3. Sample preparation for MALDI- or SALDI-TOF MS.

The CHCA matrix (10 mg) was dissolved in 0.1% TFA in water/acetonitrile (1/1, v/v). MOFs (1 mg) and SBA-15 (1 mg) were dispersed separately in a 100 μL solution of ethanol and sonicated for 5 min each.

Dried droplet method: 1 μL solution of PAHs was pipetted onto the stainless steel target and left in the air for 5-10 min for solvent evaporation. 1 μL of the suspension (CHCA, MOFs or SBA-15) or AuNPs (size for 3.5-, 14-, 33-nm;150 pM) was then pipetted onto the layer of PAHs sample quickly. It was left in the air at room temperature for 5-10 min to form a thin layer, and for further analysis by MALDI- or SALDI-TOF MS.

Two-layer method: 1 μL of CHCA suspension was deposited onto the plate and

dried in the air. A solution containing CHCA (1 μL) and PAHs (1 μL) was depoisted onto a thin layer of predeposited/dried matrix seed.

On probe remix: the deposited PHAs (1 μL) droplet is immediately overlaid with the CHCA solution (1 μL) before letting the mixture air-dry at room temperature.

4. Solid-phase extraction (SPE) prior to SALDI-TOF MS analysis with MOF as the adsorbent and matrix (scheme S1†).

MIL-100(Fe)(1 mg) was suspended in ethanol (100 μL). After sonication for 5 min, the suspension (2 μL) was pipetted immediately into 500 μL of local river water sample spiked with 1 μg/mL PAHs. The mixture was then vortexed for 30 min. After centrifugation at 6000 rpm for 30 min, the supernatant was removed, and the MIL-100(Fe) pellets on which the analytes were enriched was resuspended in ethanol (2 μL) and was pipetted onto the sample target. The sample target was left at room temperature for 10-15 min for evaporation of the solvent and for further analysis by SALDI-TOF MS.

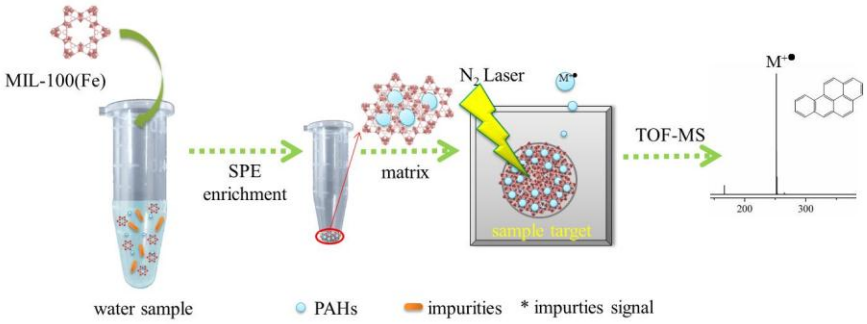

Scheme S1 MIL-100(Fe) used as an adsorbent for solid-phase extraction of PAHs and as matrix for SALDI-MS analysis.

5. Mass Spectrometry

Autoflex III MALDI-TOF mass spectrometer (Bruker Daltonics) equipped with a 337 nm Nd:YAG- laser and with a repetition rate of up to 50 Hz was used in the MS system operated in the reflection mode. Instead of anti-inflammatory drug was detected in reflectron negative-ion mode, other analytes were detected in positive-ion mode. The available accelerating voltages existed in the range from +20 to -20 kV. To obtain good resolution and signal-to-noise (S/N) ratios, the laser power was adjusted

to slightly above the threshold, and each mass spectrum was generated by averaging 500 laser pulses. All data are derived from five replicated experiments.

6. Synthesis of 3.5, 14, 33- nm Au NPs

The 3.5 nm AuNPs was synthetic according to H.-T. Chang *et al.*(ref. S7). Briefly, a 20 mL aqueous solution containing 0.25 mM trisodium citrate and 0.25 nM $HAuCl_4$ was prepared in breaker and stirred. Next, ice-cold 0.1 M NaBH4 (0.6 mL) was added into the solution immediately, then the solution turned to purple color. The synthesis procedure of 14 nm Au was according to H.-T. Chang *et al.*(ref. S8). Briefly, trisodium citrate (4 mM, 50 mL) was heated to boil under reflux with stirring in a round-bottom flask, and then $HAuCl_4$ (30 mM, 1.67 mL) was rapidly added into the boiled solution for another 3 mins heating, during which time the solution changed color from pale yellow to purple and then to wine-red. The 33 nm Au was synthesized according to H.-T. Chang *et al* (ref. S7). Briefly, 50 mL of 0.01% $HAuCl_4$ was heated to boil under reflux, then 1 mL of 1% trisodium citrate was added rapidly. Until the solution turned to blue, continue heating for another 2 mins. During the time the souultion changed to purple. UV-vis spectrometer was used to examine the absorbance of the AuNPs in the citrate solution. The maximum absorption wavelength of 3.5, 14, and 33-nm Au was at 503, 518, and 526 nm, respectively, indicated the formation of AuNPs (Figure S2f).

7. Synthesis of SBA-15

SBA-15 was synthesized according to the literature with slight modification (ref. S9). Briefly, 4.0 g of Pluronic P123 was dissolved in 150 g of 2 M HCl solution with stirring at 35 °C. Then 8.50 g of TEOS was added into that solution with stirring at 25°C for 20 h, and the mixture was aged at 80 °C overnight without stirring. The

white powder product was recovered, washed, and vacuum-dried. Calcination was carried out by slowly increasing temperature from room temperature to 500 °C for 8 h and heating at 500 °C for 6 h. The characteristics of SBA-15 are shown in Figure S1 including powder X-ray distribution, N_2 adsorption-desorption isotherm, pore size distribution, and TEM image.

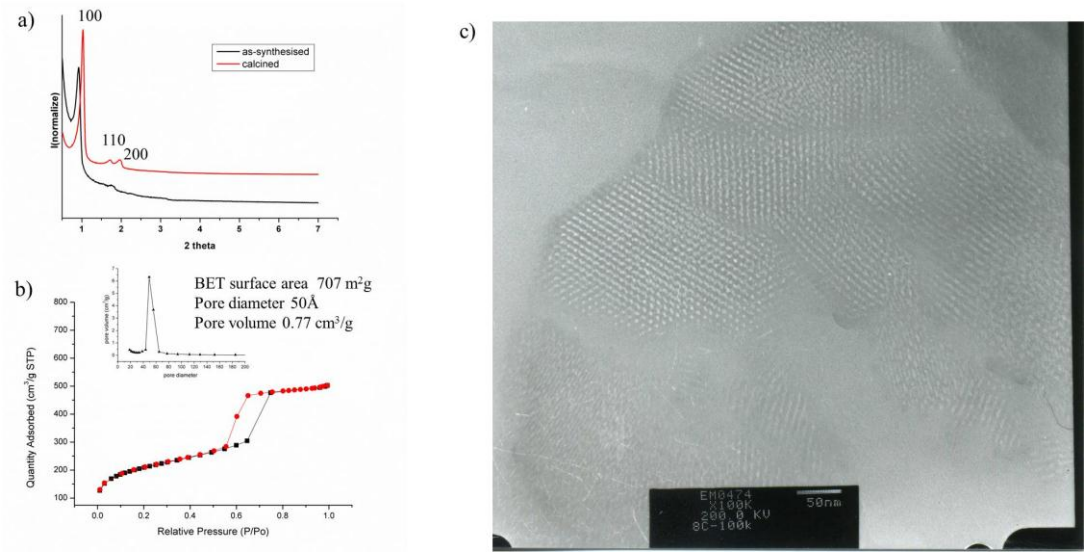

Figure S1 Characterization of SBA-15. a) PXRD pattern; b) N_2 adsorption-desorption isotherm and pore size distribution curves (inset); c) TEM image.

8.

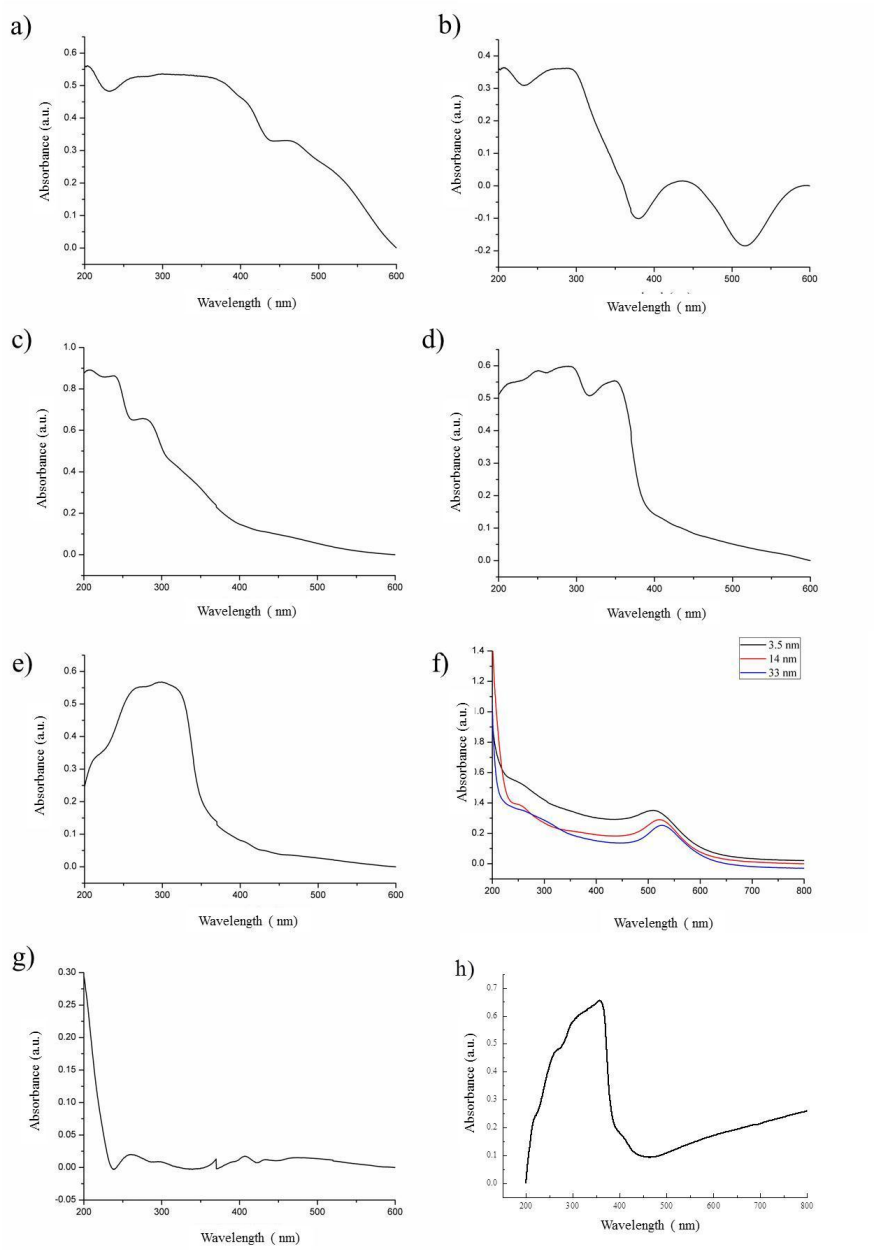

Figure S2 UV-visible spectra of MOFs a) MIL-100(Fe); b) MIL-100(Cr); c) MIL-100(Al); d) DUT-4; e) DUT-5; f) AuNPs; g) SBA-15; h) CYCU-3.

9.

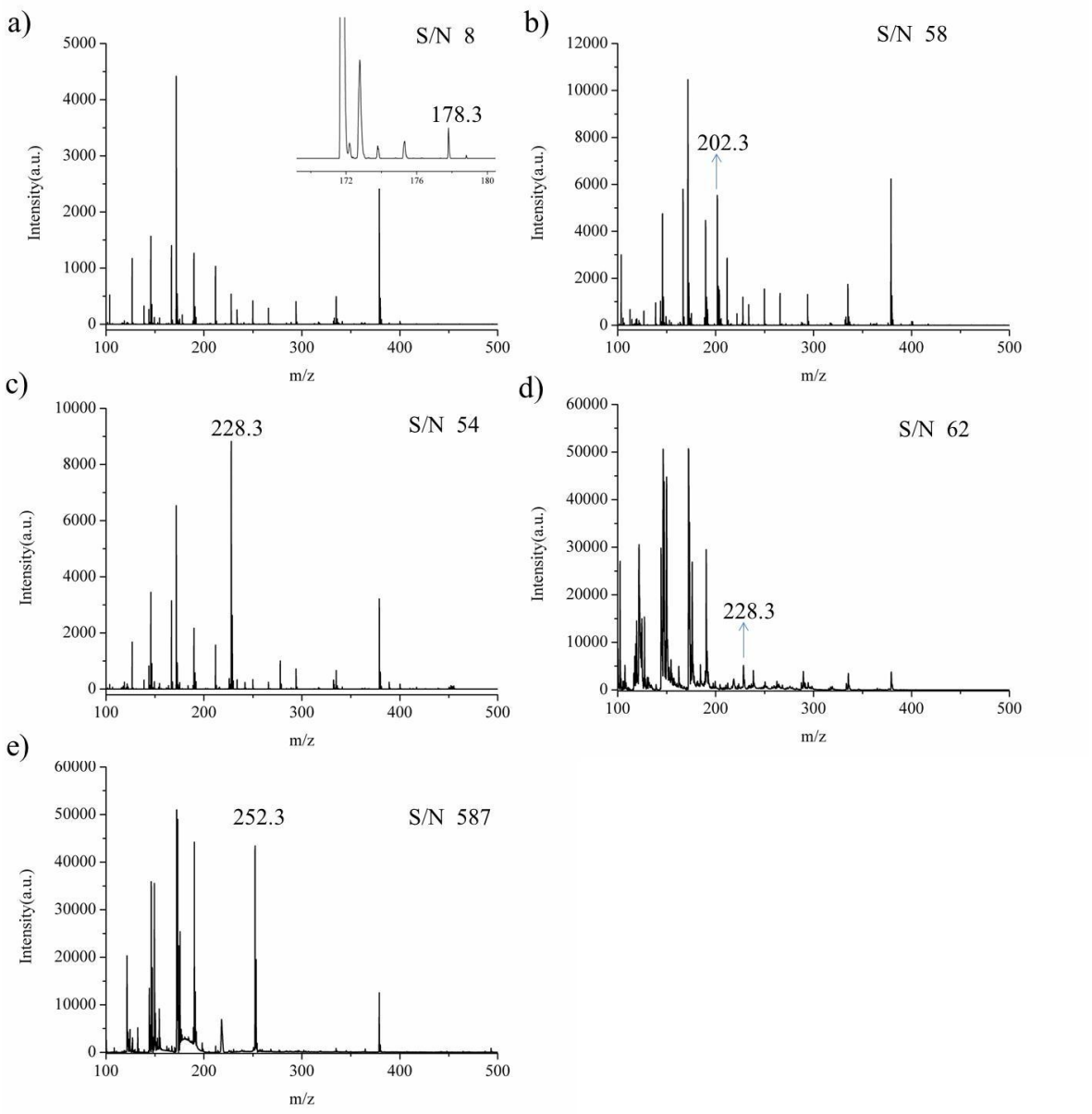

Figure S3 MALDI-MS spectra of PAHs using CHCA as matrix. a) Ant (m/z 178.3, $M^{+\bullet}$); b)Pyr (m/z 202.3, $M^{+\bullet}$); c) BaA (m/z 228.3, $M^{+\bullet}$); d) Chr (m/z 228.3, $M^{+\bullet}$); e) BaP (m/z 252.3, $M^{+\bullet}$). PAHs concentration: 100 μg/mL.

10.

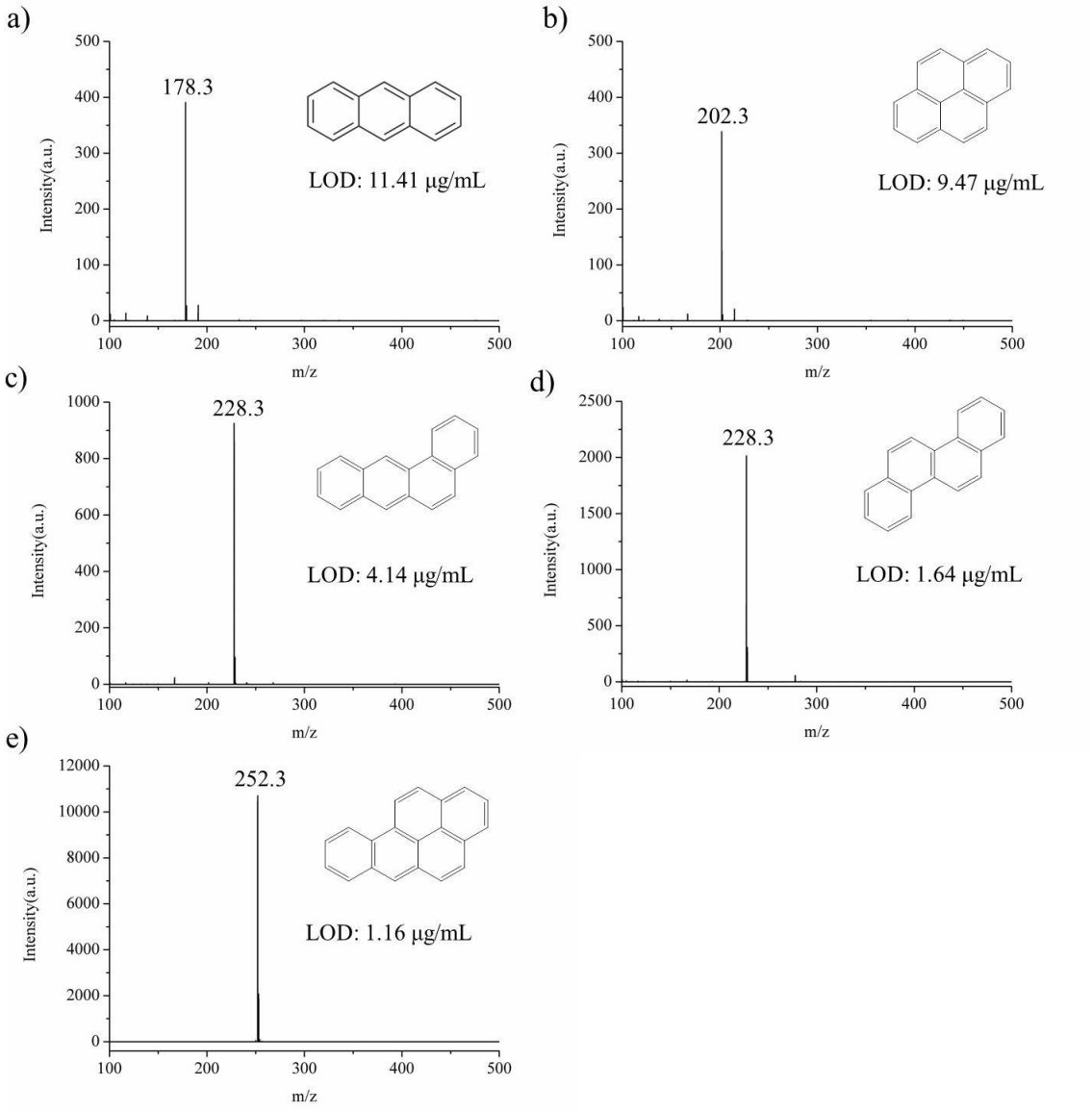

Figure S4 SALDI-MS spectra of PAHs using MIL-100(Fe) as matrix. a) Ant (m/z 178.3, $M^{+\bullet}$); b)Pyr (m/z 202.3, $M^{+\bullet}$); c) BaA (m/z 228.3, $M^{+\bullet}$); d) Chr (m/z 228.3, $M^{+\bullet}$); e) BaP (m/z 252.3, $M^{+\bullet}$). PAHs concentration: 100 μg/mL.

11.

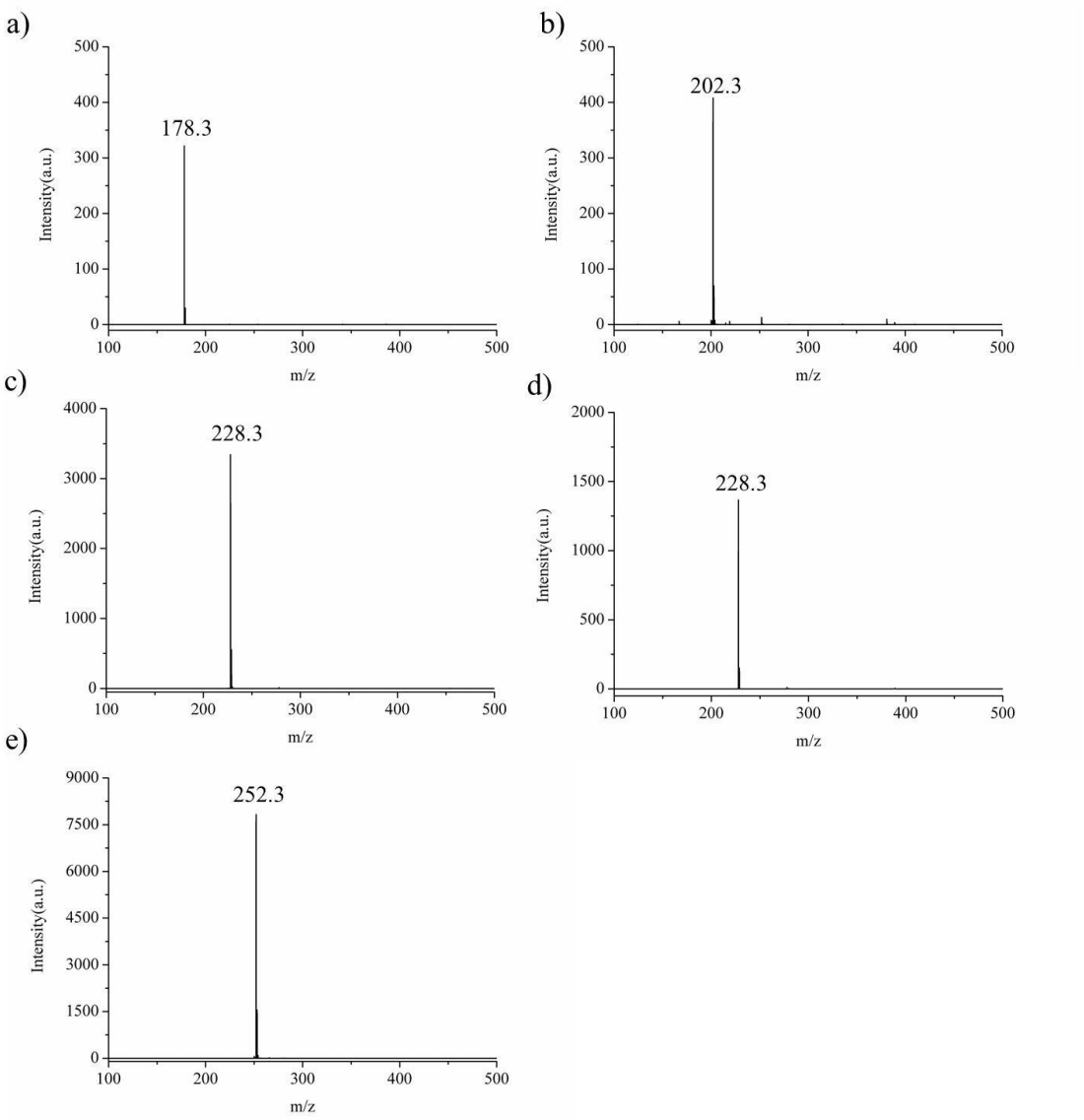

Figure S5 SALDI-MS spectra of PAHs using MIL-100(Cr) as matrix. a) Ant (m/z 178.3, $M^{+\bullet}$); b)Pyr (m/z 202.3, $M^{+\bullet}$); c) BaA (m/z 228.3, $M^{+\bullet}$); d) Chr (m/z 228.3, $M^{+\bullet}$); e) BaP (m/z 252.3, $M^{+\bullet}$). PAHs concentration: 100 μg/mL.

12.

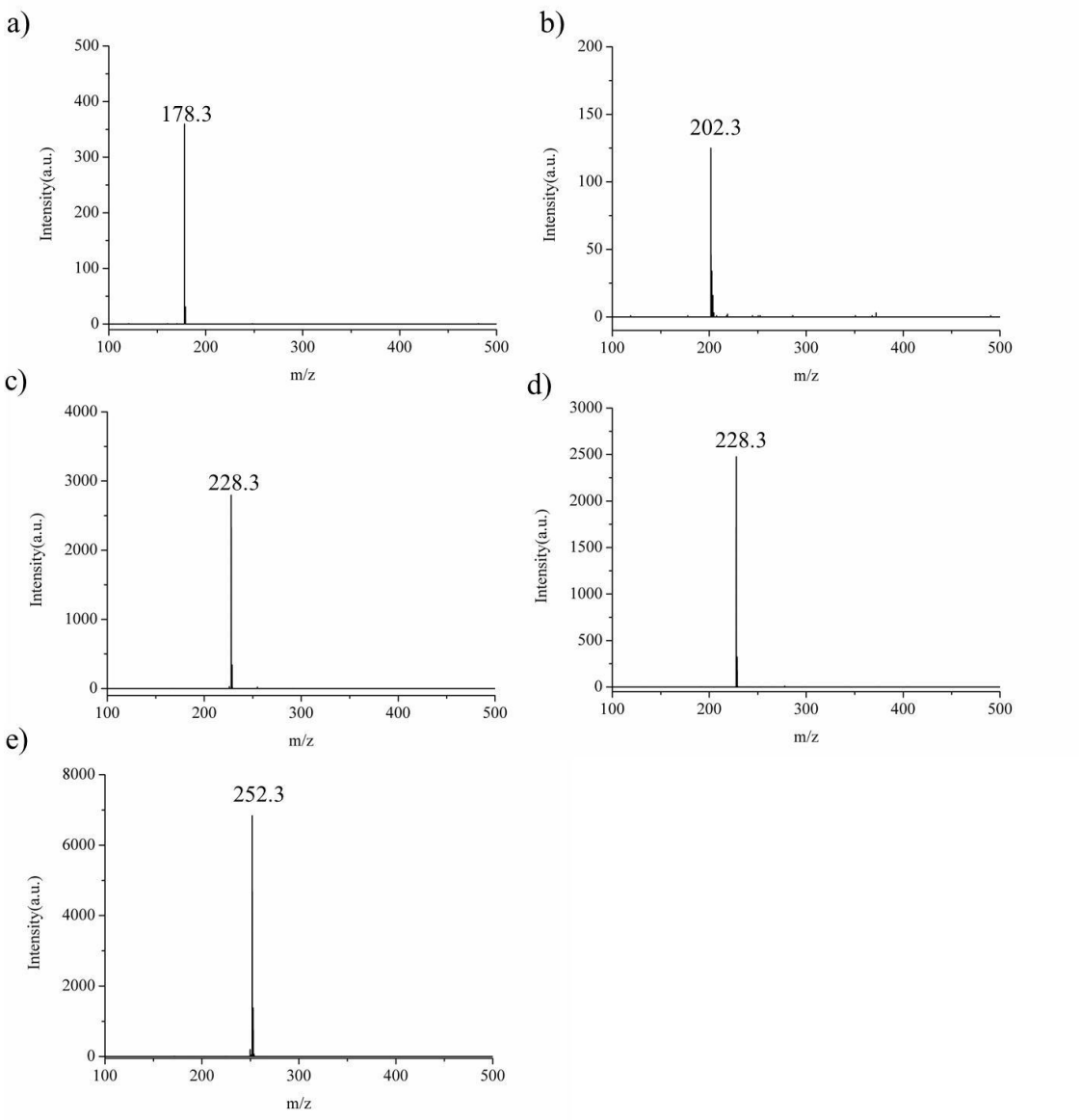

Figure S6 SALDI-MS spectra of PAHs using MIL-100(Al) as matrix. a) Ant (m/z 178.3, $M^{+\bullet}$); b)Pyr (m/z 202.3, $M^{+\bullet}$); c) BaA (m/z 228.3, $M^{+\bullet}$); d) Chr (m/z 228.3, $M^{+\bullet}$); e) BaP (m/z 252.3, $M^{+\bullet}$). PAHs concentration: 100 μg/mL

13.

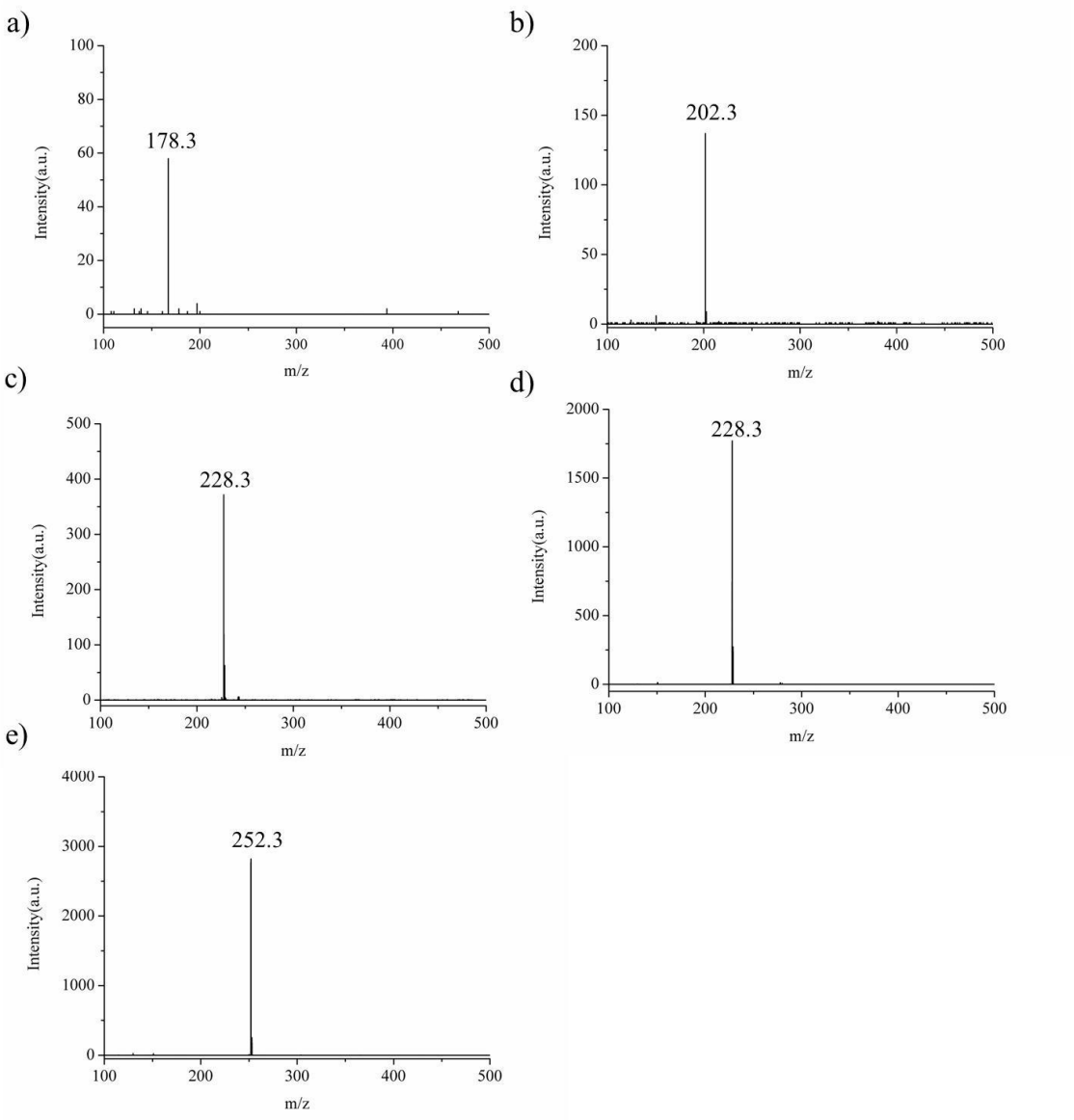

Figure S7 SALDI-MS spectra of PAHs using MIL-101(Cr) as matrix. a) Ant (m/z 178.3, $M^{+\bullet}$); b)Pyr (m/z 202.3, $M^{+\bullet}$); c) BaA (m/z 228.3, $M^{+\bullet}$); d) Chr (m/z 228.3, $M^{+\bullet}$); e) BaP (m/z 252.3, $M^{+\bullet}$). PAHs concentration: 100 μg/mL.

14.

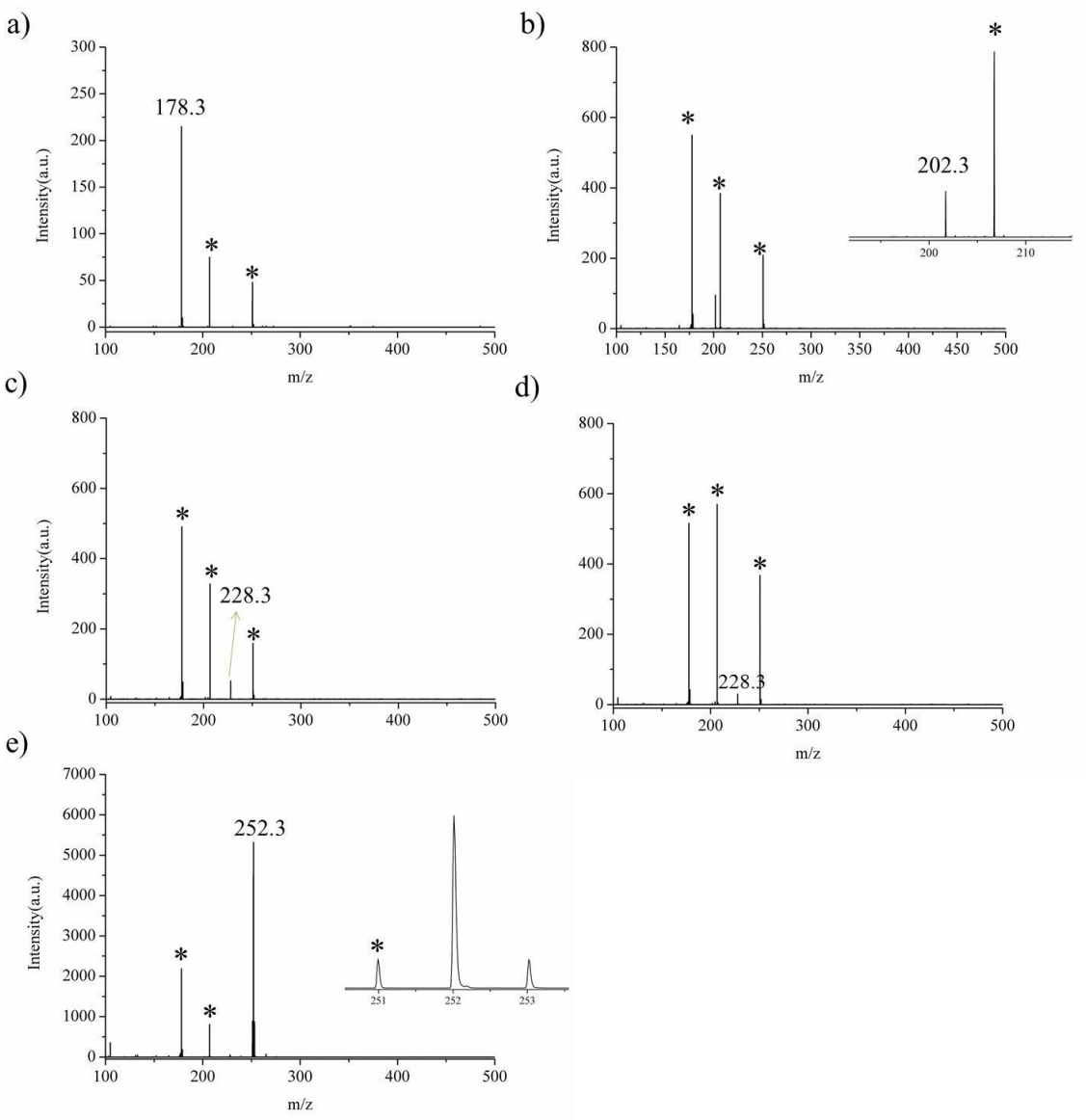

Figure S8 SALDI-MS spectra of PAHs using CYCU-3(Al) as matrix. a) Ant (m/z 178.3, $M^{+\bullet}$); b)Pyr (m/z 202.3, $M^{+\bullet}$); c) BaA (m/z 228.3, $M^{+\bullet}$); d) Chr (m/z 228.3, $M^{+\bullet}$); e) BaP (m/z 252.3, $M^{+\bullet}$). PAHs concentration: 100 μg/mL. *The signals were identified as the precursor ions for CYCU-3 syntheses.

15.

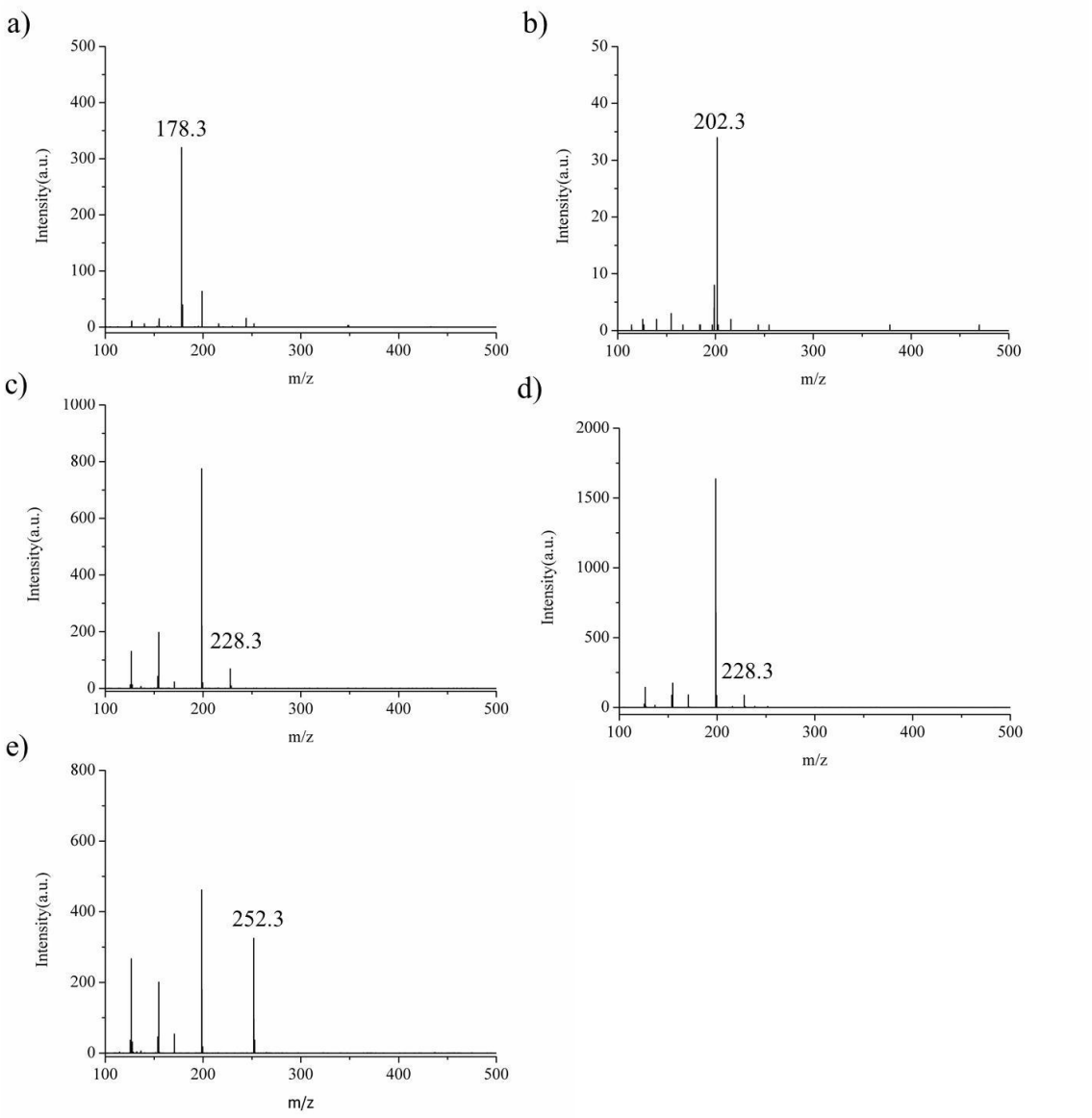

Figure S9 SALDI-MS spectra of PAHs using DUT-4 as matrix. a) Ant (m/z 178.3, $M^{+\bullet}$); b)Pyr (m/z 202.3, $M^{+\bullet}$); c) BaA (m/z 228.3, $M^{+\bullet}$); d) Chr (m/z 228.3, $M^{+\bullet}$); e) BaP (m/z 252.3, $M^{+\bullet}$). PAHs concentration: 100 μg/mg.

16.

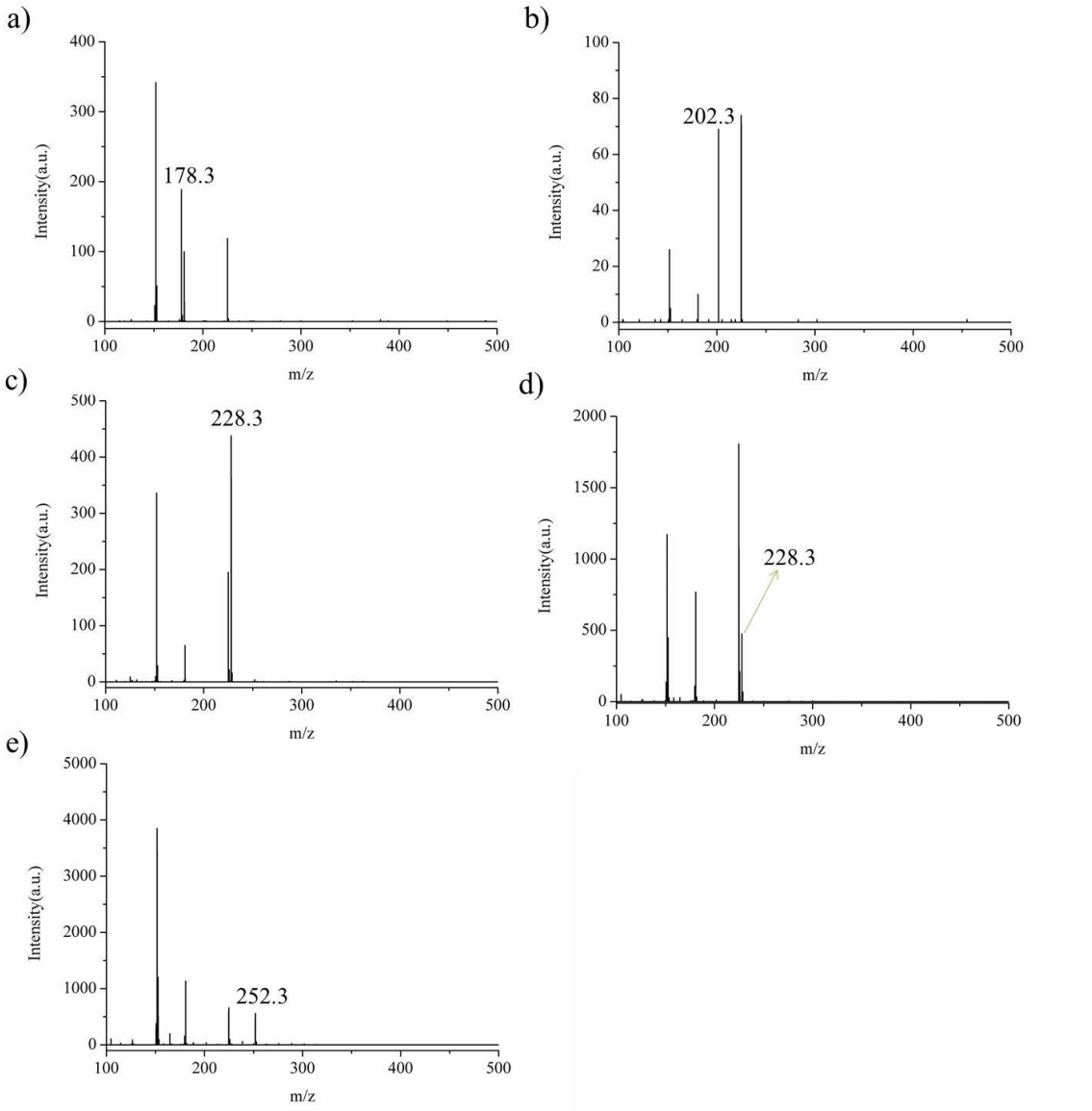

Figure S10 SALDI-MS spectra of PAHs using DUT-5 as matrix. a) Ant (m/z 178.3, $M^{+\bullet}$); b)Pyr (m/z 202.3, $M^{+\bullet}$); c) BaA (m/z 228.3, $M^{+\bullet}$); d) Chr (m/z 228.3, $M^{+\bullet}$); e) BaP (m/z 252.3, $M^{+\bullet}$). PAHs concentration: 100 μg/mL.

17.

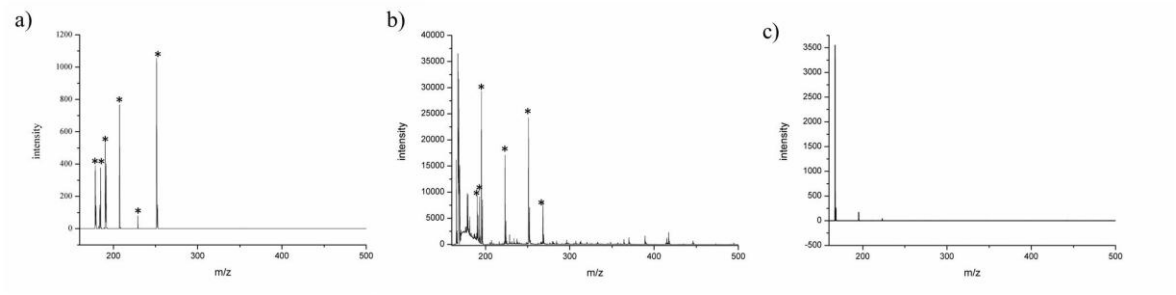

Figure S11 Laser induced ionization mass spectra of a) CYCU-3; b) organic ligands (4,4‘-stilbenedicarboxylic acid (SDC)) of CYCU-3; c) aluminum source of CYCU-3. Matrix concentration: 10 μg/μL. *The signals were identified as the precursor ions for CYCU-3 syntheses.

18.

In this context, various concentrations of MIL-100(Fe) matrix (10^{-2}-10^{3} μg/μL) was used to analyze benzo[a]pyrene and evaluation on its effect showed that increasing the matrix concentration also increased the signal intensity up to 10^{2}, while further increase resulted in decreased analyte intensity probably due to matrix aggregation. Then, the optimized matrix concentration was used to analyze a mixture of these PAHs to demonstrate the capability of the matrix in resolving multi-analyte analysis in a single run.

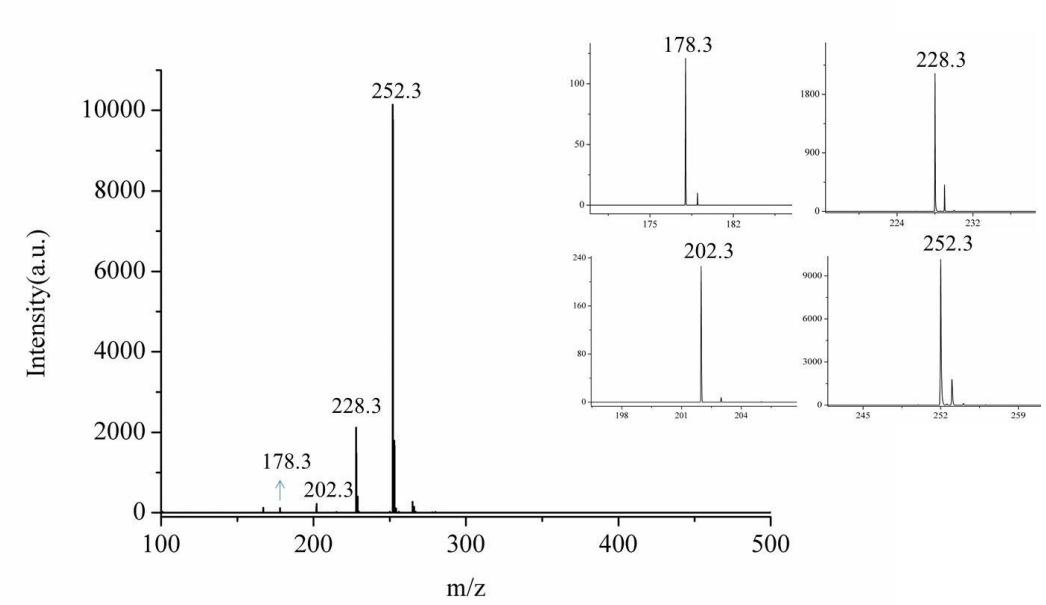

Figure S12 SALDI-MS spectra of 4 PAHs using MIL-100(Fe) as matrix. Ant (m/z 178.3, $M^{+\bullet}$), Pyr (m/z 202.3, $M^{+\bullet}$), Chr (m/z 228.3, $M^{+\bullet}$), BaA (m/z 252.3, $M^{+\bullet}$). PAHs concentration: 100 μg/mL.

19.

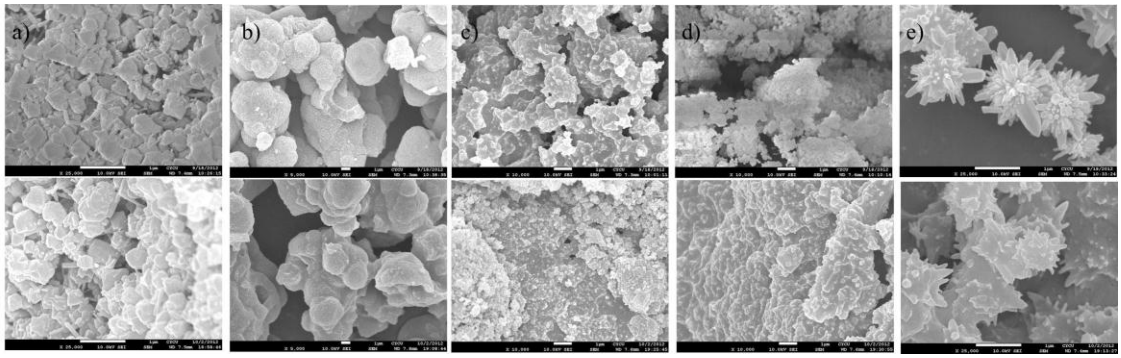

Figure S13 SEM images of as-synthesized MOFs (above) and laser irradiated MOFs (below). a) MIL-100(Al); b) MIL-100(Cr); c) DUT-4; d) DUT-5; e) CYCU-3.

20.

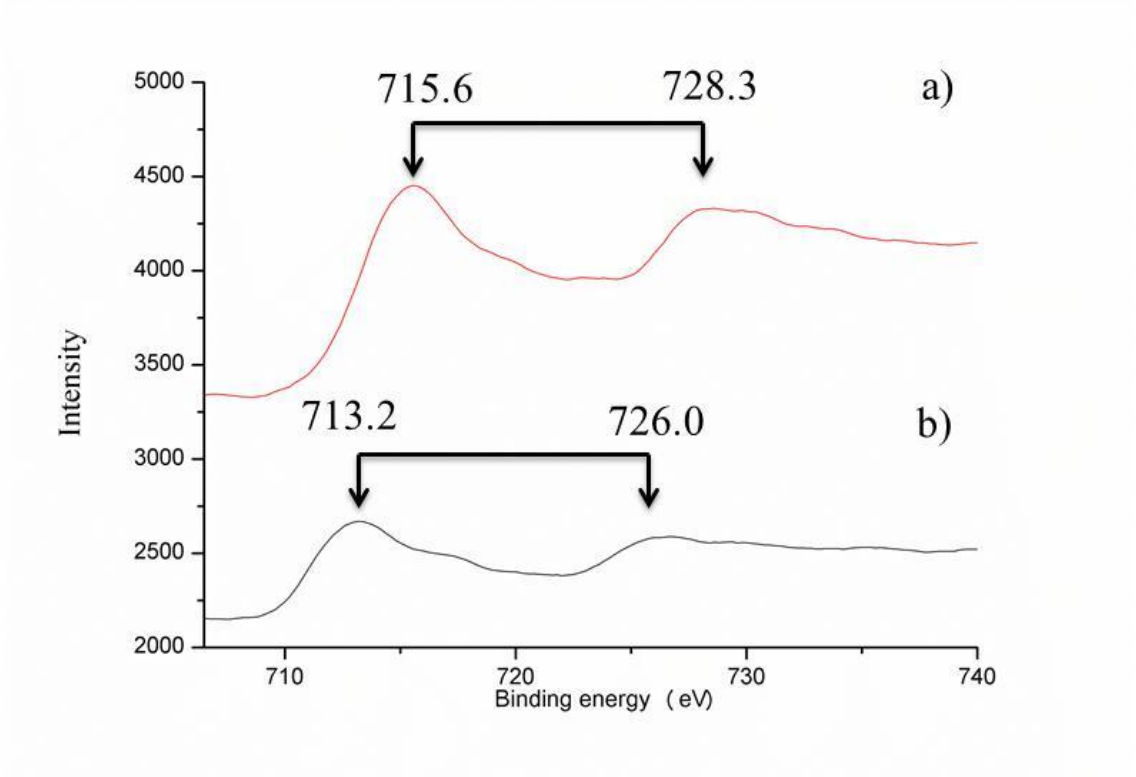

Figure S14 ESCA spectra of MIL-100(Fe) a) as-synthesized; b) after laser irradiation.

21.

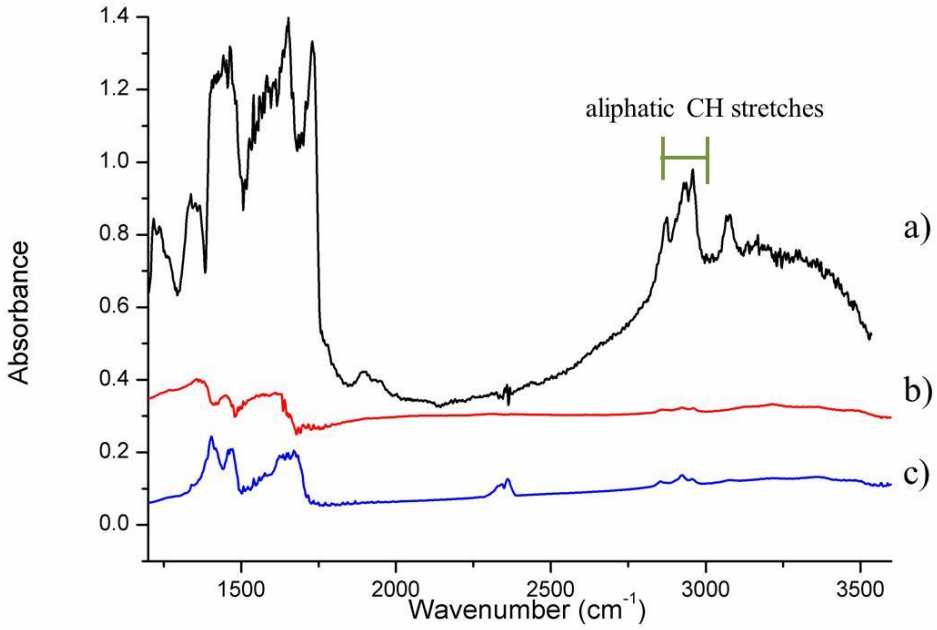

Figure S15 Micro FT-IR spectra of MIL-100 after laser irradiated MOF under SALDI-MS experiment. a) MIL-100(Fe), b) MIL-100(Al), c) MIL-100(Cr).

22.

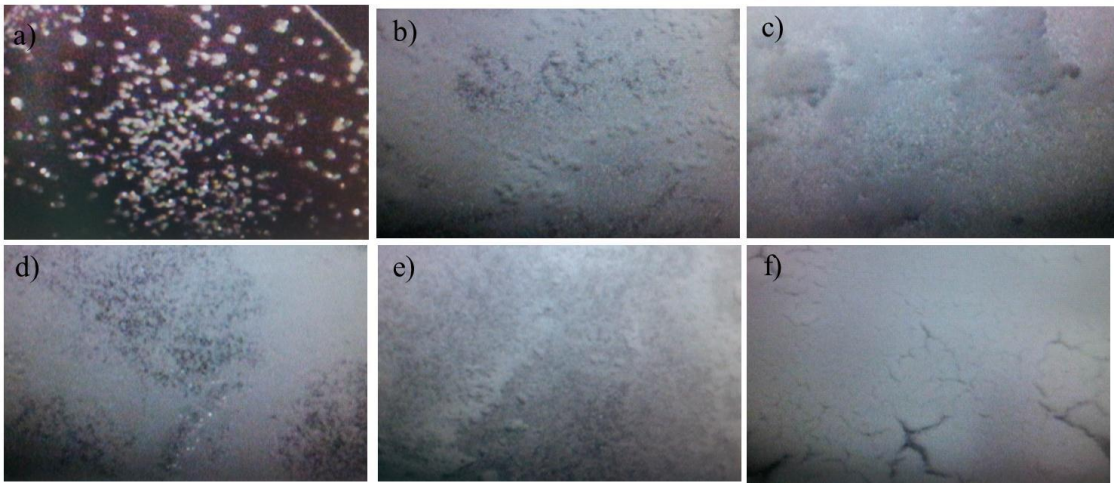

Figure S16 Optical images of a) CHCA; b) MIL-100(Fe); c) MIL-101(Cr); d)DUT-4; e) DUT-5; f) CUCY-3 dispersed on the stainless steel target after laser pulse. Matrix concentration: 10 μg/μL.

23.

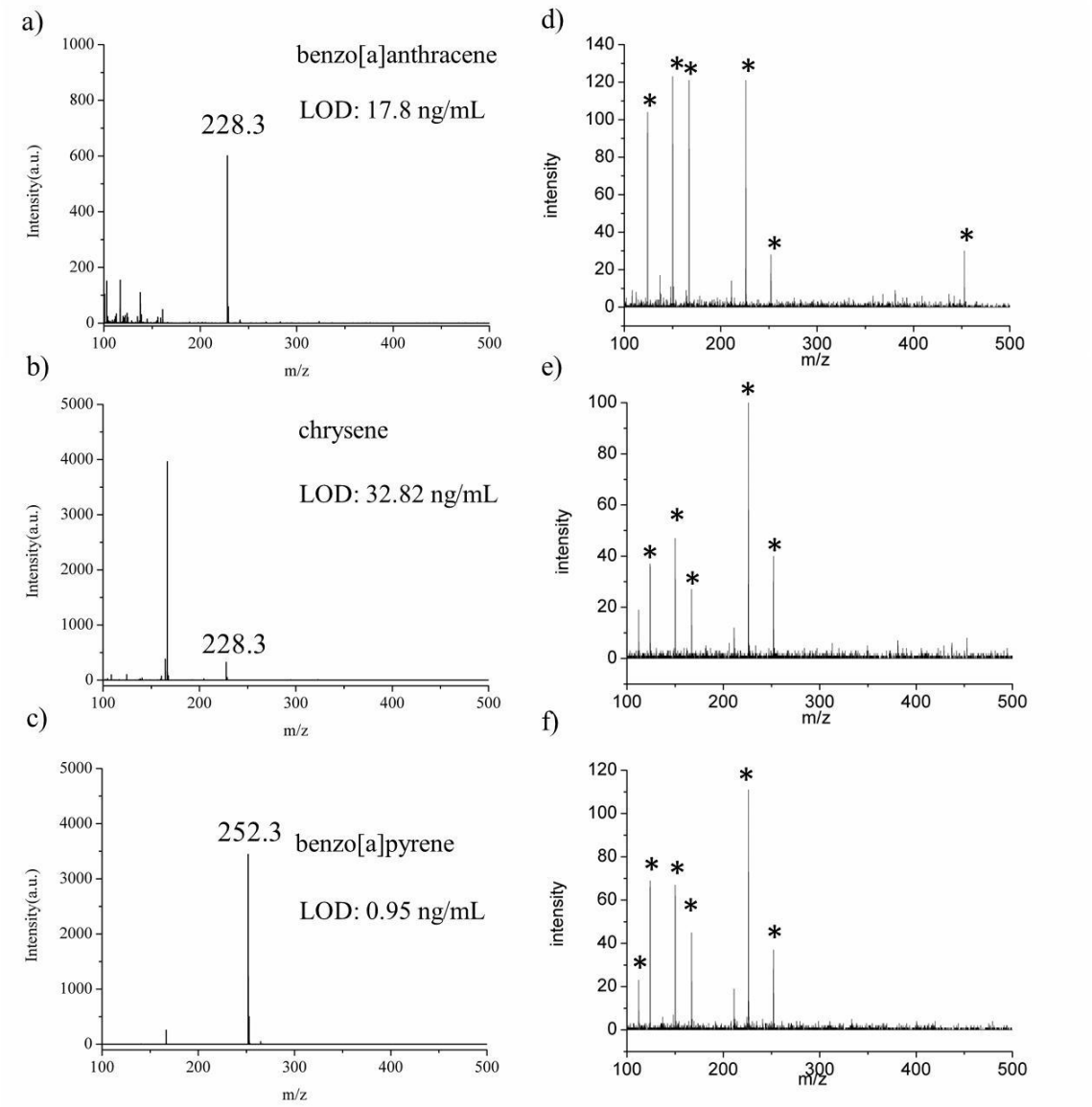

Figure S17 SALDI-MS spectra of river water samples spiked with 1μg/mL PAHs using MIL-100(Fe) as matrix and solid-phase-extraction (SPE) adsorbent. Samples were determined with SPE (a-c) and without SPE treatment (d-f). *the signal was produced from unknown components in river water sample.

24.

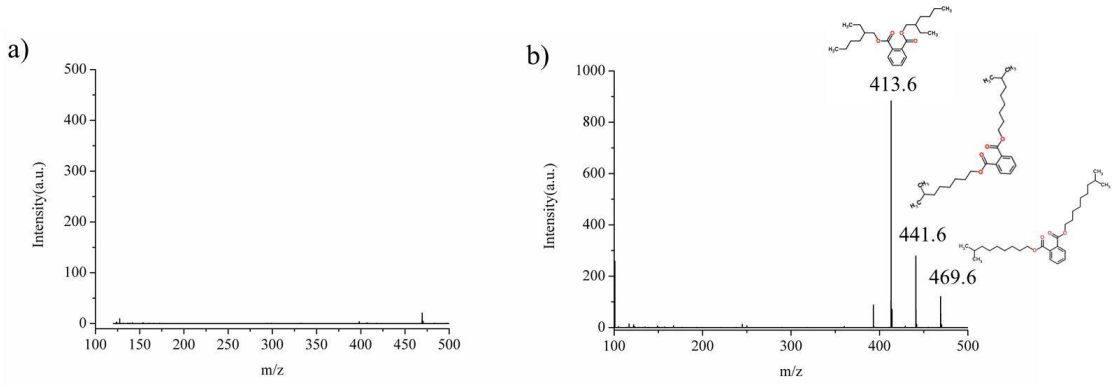

Figure S18 SALDI-MS spectra of ester compounds detected without matrix a) and with MIL-100(Fe) matrix b). (m/z 413.5, $[M+Na]^+$; m/z 441.6, $[M+Na]^+$; m/z 469.6, $[M+Na]^+$).

25.

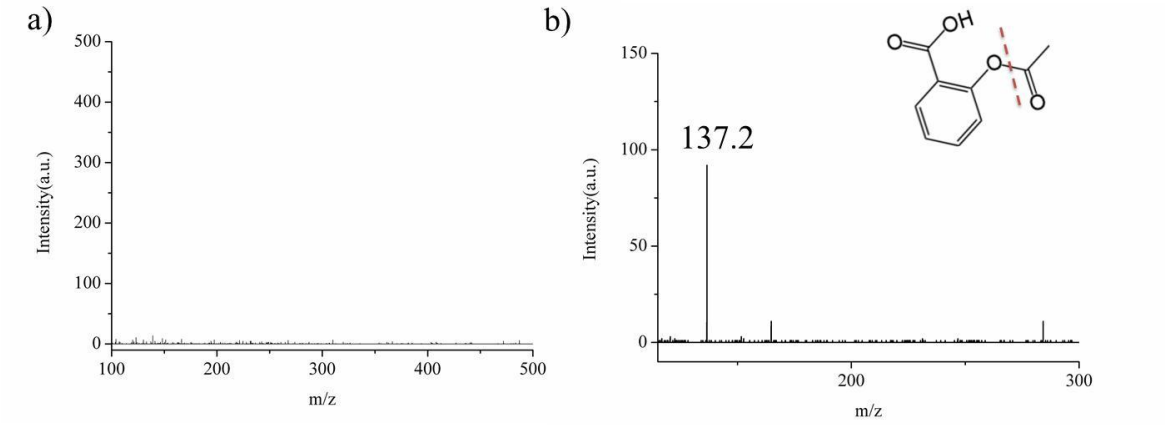

Figure S19 SALDI-MS spectra of anti-inflammatory drug (m/z 137.2, $[M-C_2H_3O]^-$) detected without matrix a) and with MIL-100(Fe) matrix b).

Mass spectra shown in Figure S18 and Figure S19 indicated no esters' and anti-inflammatory drug's signals found without MOFs (Figures S18a and S19a), while positive-ion signals of three ester compounds as well as negative-ion signals of anti-inflammatory drug were acquired with MOFs use (Figure S18b) and no background noises observed in these mass spectra. Furthermore, when using MOFs as matrix, three ester compounds detected as the $[M + Na]^+$ form (no extra sodium ion addition) that exhibits a sodium adduct mechanism (Figure S18b); anti-inflammatory drug detected as $[M- C_2H_3O]^-$ form that presents a possible deprotonation effect occurred (Figure S19b). These observations display high feasibility of using MOFs as SALDI-MS matrix for analysis of other nonpolar and polar compounds.

26.

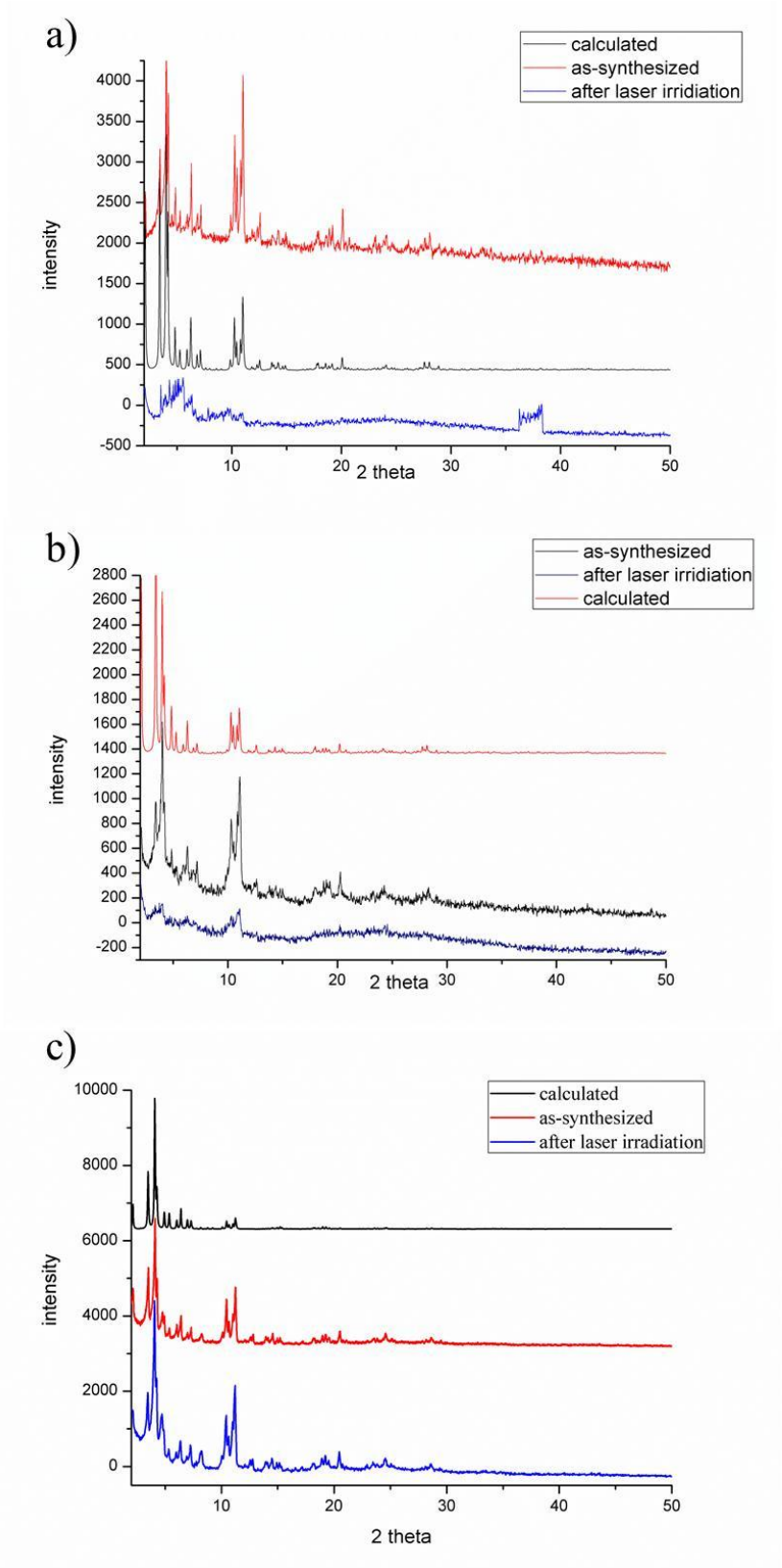

Figure S20 powder X-ray diffraction (PXRD) patterns of a) MIL-100(Fe); b) MIL-100(Cr); c) MIL-100(Al). Laser intensity: 20 mW.

27.

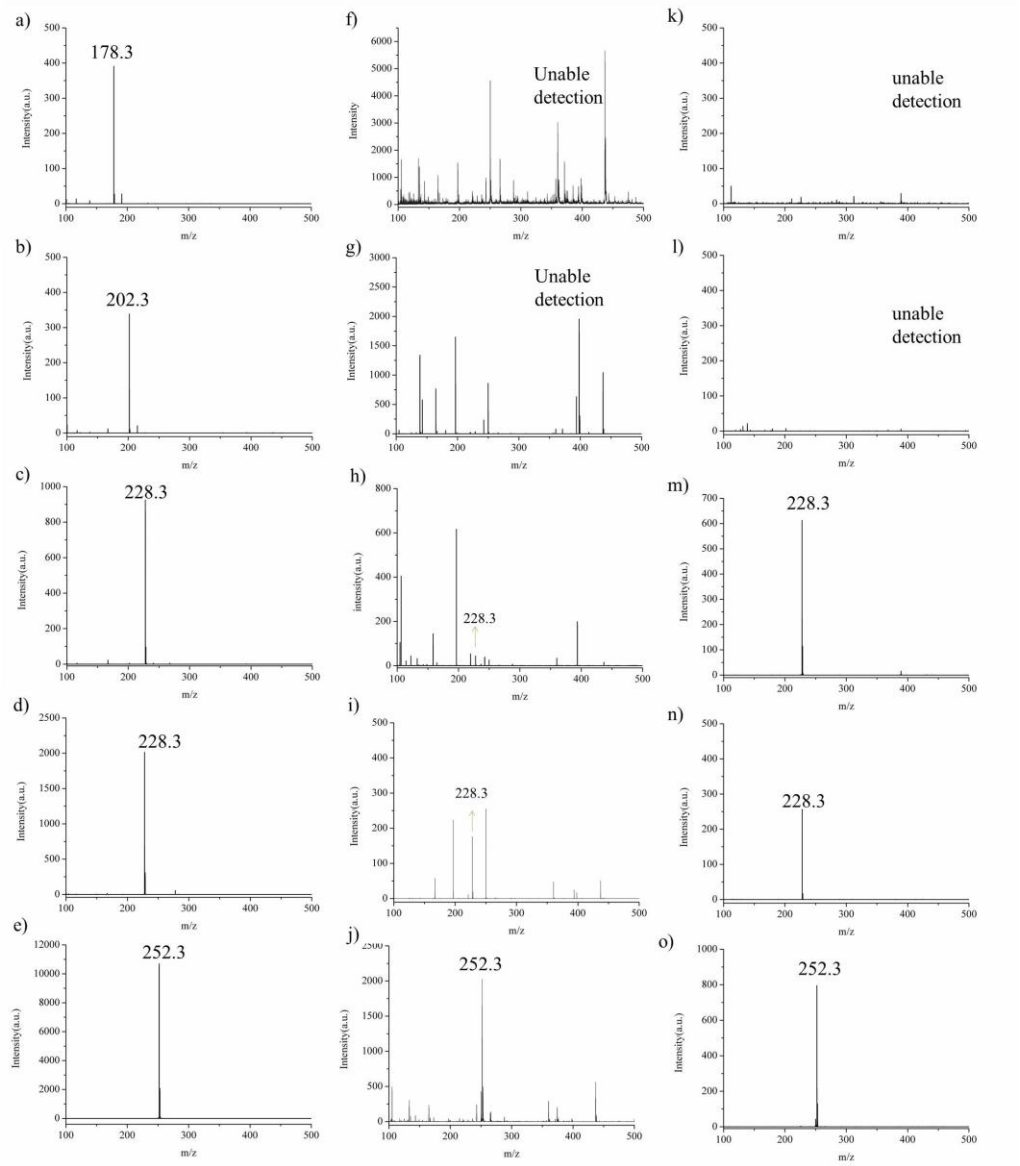

Figure S21 SALDI-MS spectra of PAHs using different nanoparticles as matrix. a-e) MIL-100(Fe); f-j) 14-nm Au; k-o) SBA-15. a, f, k) Ant (m/z 178.3, $M^{+\bullet}$); b, g, l) Pyr (m/z 202.3, $M^{+\bullet}$); c, h, m) BaA (m/z 228.3, $M^{+\bullet}$); d, i, n) Chr (m/z 228.3, $M^{+\bullet}$); e, j, o) BaP (m/z 252.3, $M^{+\bullet}$). PAHs concentration: 100 μg/mL. Laser power:56%.

28.

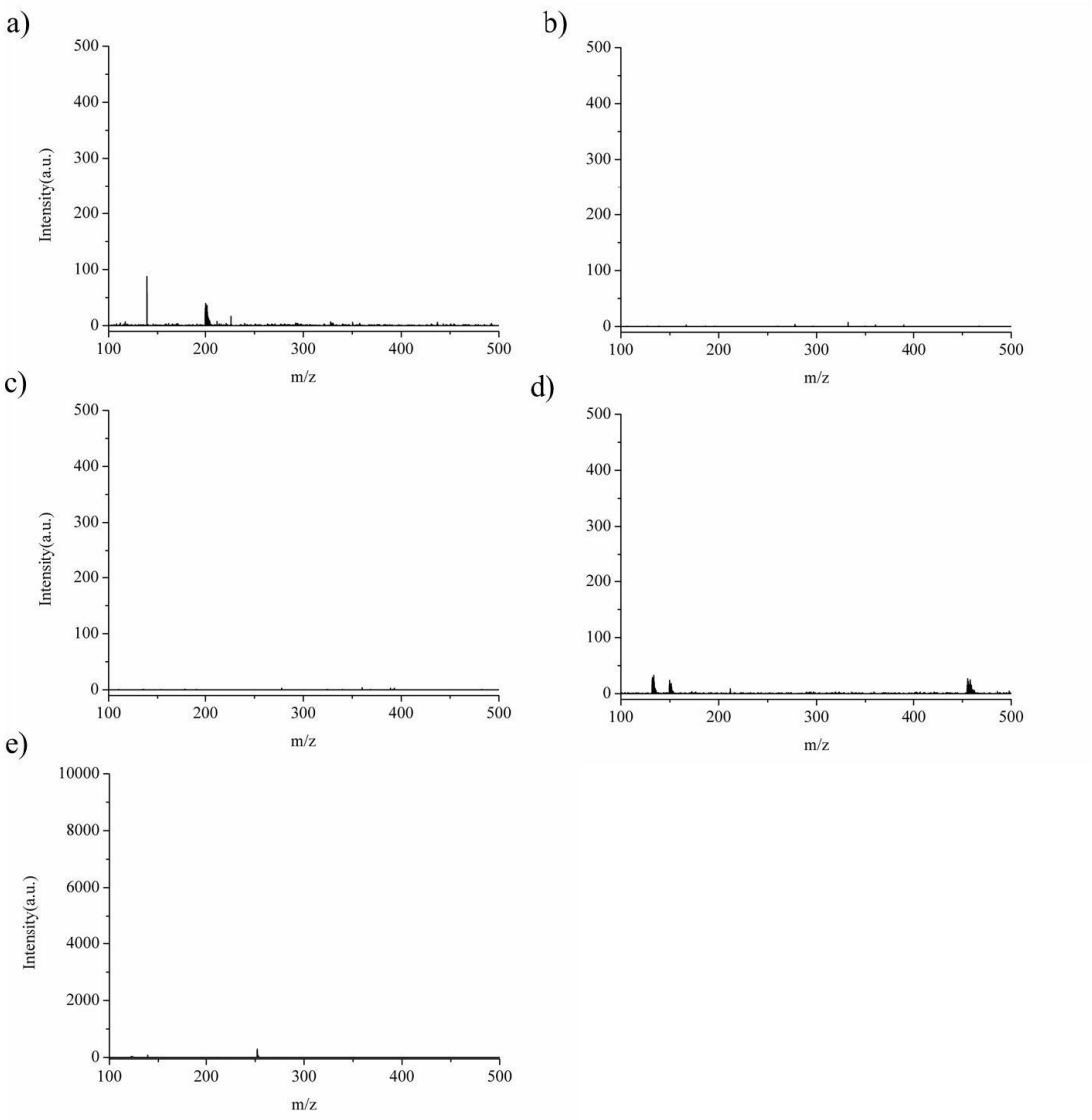

Figure S22 Mass spectra of laser desorption/ionization of PAHs without matrixes. a) Ant; b) Pyr; c) BaA; d) Chr; e) BaP. PAHs concentration: 100 μg/mL.

29.

In the absence of the matrix, some PAHs that carry more benzene rings, such as benzo[ghi]perylene (m/z, 276.3), could produce their molecular ion signals via laser irradiation because of the charge transfer effect, however, the use of MIL-100(Fe) as matrix enhances greatly their signal intensity and reproducibility.

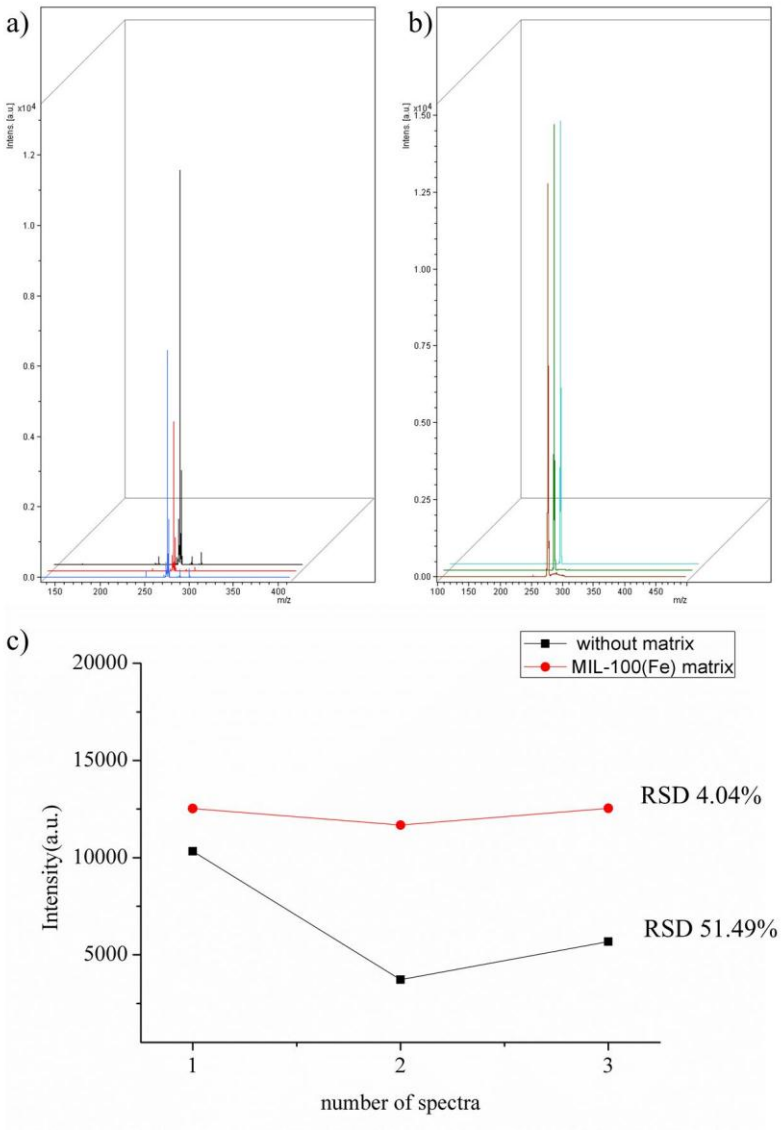

Figure S23 The reproducibility of mass intensity for laser desorption/ionization analysis of benzo[ghi]perylene (m/z, 276.3). a) without matrix; b) MIL-100(Fe) matrix. Concentration: 100 μg/mL.

30.

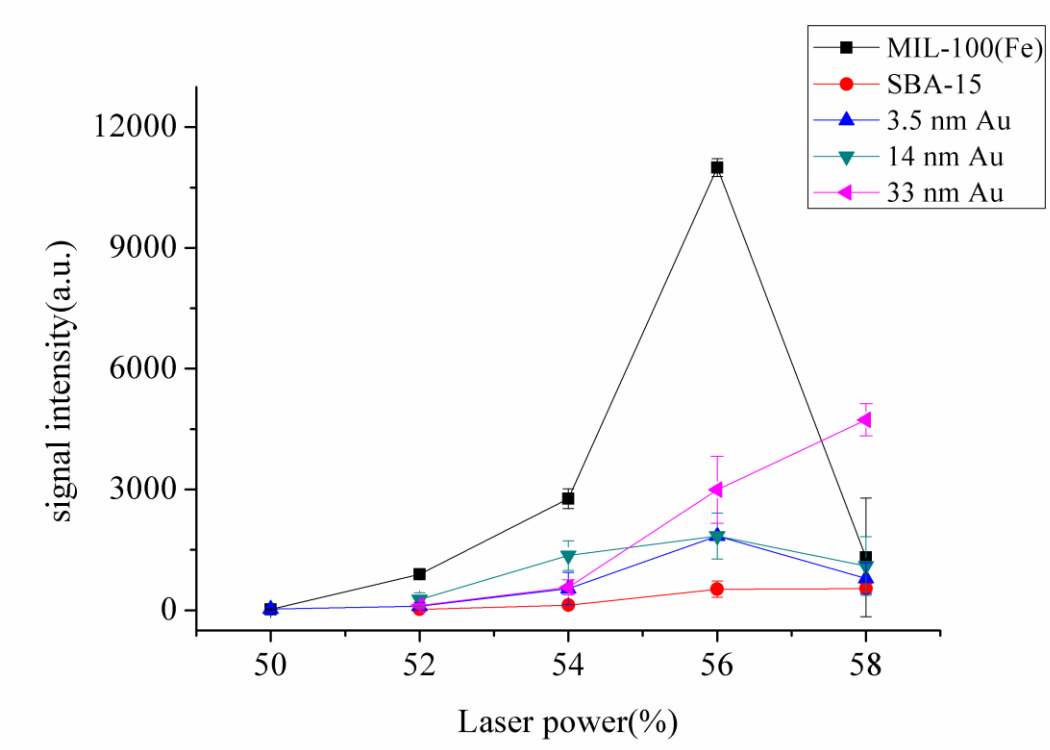

Figure S24 Laser power effects on SALDI-MS analysis of benzo[a]pyrene using MOFs and NPs as matrixes. Each data was collected by 5 spectra.

31.

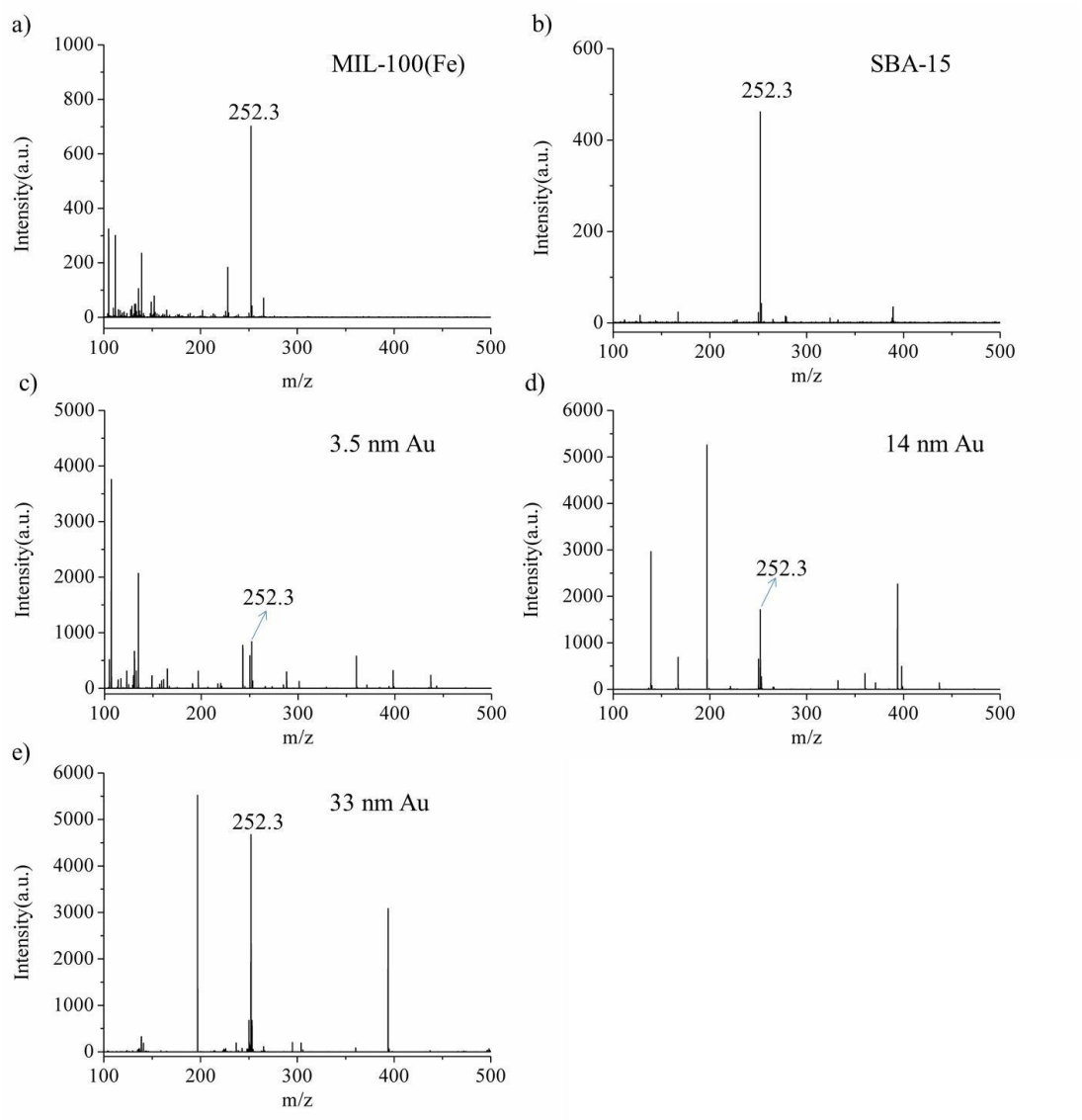

Figure S25 SALDI-MS analysis of benzo[a]pyrene via a) MIL-100(Fe); b) SBA-15; c) 3.5 nm Au; d) 14 nm Au; e) 33 nm Au as matrix. Laser power: 58%.

32.

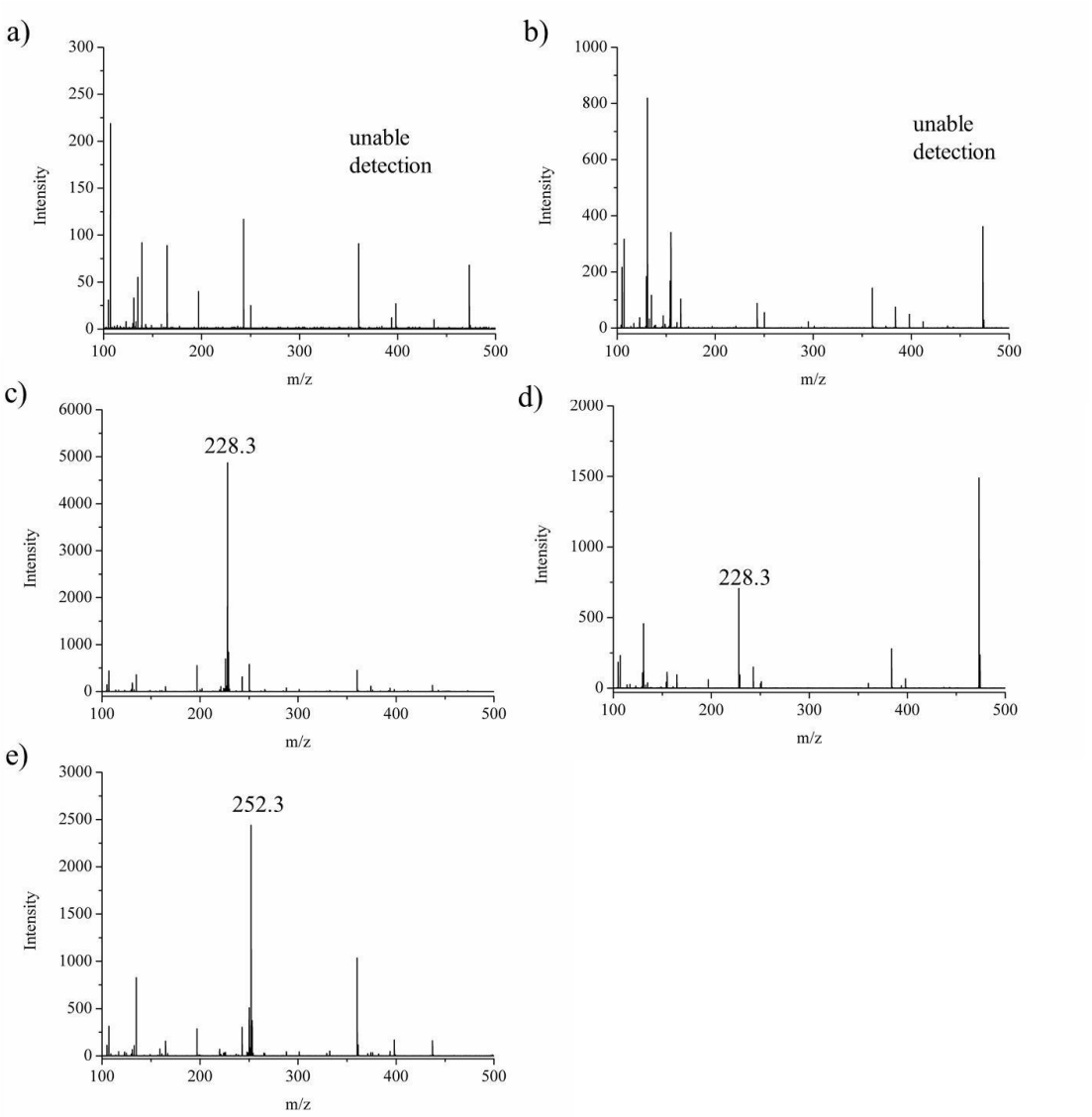

Figure S26 SALDI-MS spectra of PAHs using 3.5 nm Au as matrix. a) Ant (m/z 178.3, $M^{+\bullet}$); b)Pyr (m/z 202.3, $M^{+\bullet}$); c) BaA (m/z 228.3, $M^{+\bullet}$); d) Chr (m/z 228.3, $M^{+\bullet}$); e) BaP (m/z 252.3, $M^{+\bullet}$). PAHs concentration: 100 μg/mL. Laser power: 56%

33.

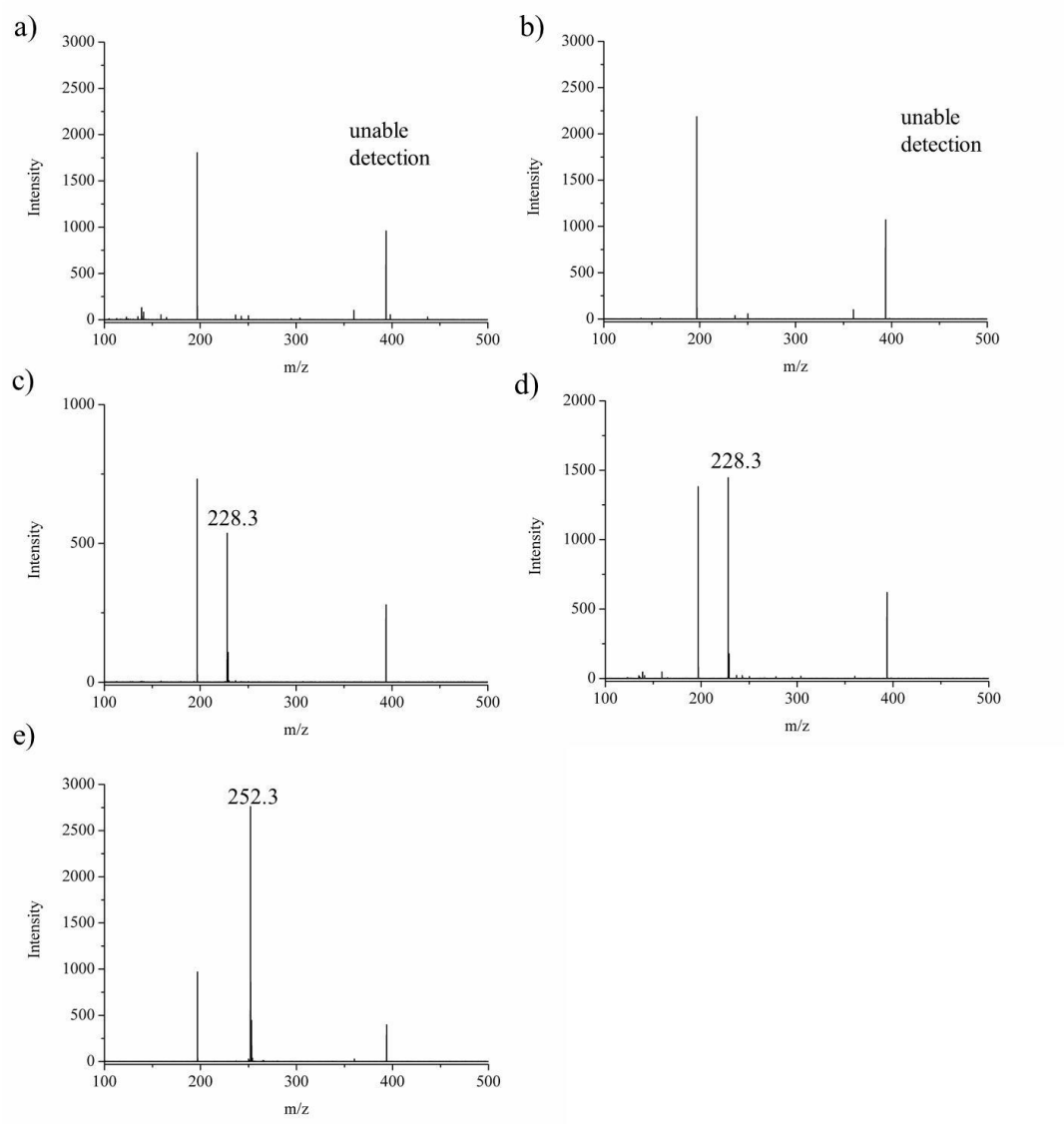

Figure S27 SALDI-MS spectra of PAHs using 33 nm Au as matrix. a) Ant (m/z 178.3, $M^{+\bullet}$); b)Pyr (m/z 202.3, $M^{+\bullet}$); c) BaA (m/z 228.3, $M^{+\bullet}$); d) Chr (m/z 228.3, $M^{+\bullet}$); e) BaP (m/z 252.3, $M^{+\bullet}$). PAHs concentration: 100 μg/mL. Laser power: 56%

In this context, the laser power ranged of 50% to 58% were used for SALDI-MS analysis of benzo[a]pyrene with different NPs (3.3-, 14-, 35-nm Au, SBA-15) and MOFs as matrixes. As shown in the profiles in Figure S24, there were no signals detected in all test matrixes when 50% laser power was used, which indicated a very weak laser intensity to ionize PAHs. The signal intensity of benzo[a]pyrene increased at laser power of 52% to 56% for each matrix, but was slightly decreased at 58% laser

power except for 33-mn Au. On the other hand, with 58% laser irradiation obvious background noises were produced in all matrixes possibly due to matrix ionization with this laser energy (Figure S25) (Rapid Commun. Mass Spectrom., 2007, 21, 837). Further examination of the profiles shown in Figure 3a (56% laser power) indicated that the usage of MOFs as matrix is capable of detecting five test PAHs, but only three PAHs detected either in AuNPs (Figure S26, 27) or SBA-15 (Figure S21(k-o)), the same results obtained even when laser power was increased to 80% (data not shown). Considering the signal intensity and background noise observed from Fig. 3a, Fig.S24 and S25, 56% laser power was chosen as the optimal condition for all other SALDI-MS experiments presented in this study.

34.

Table S1 Reproducibility of signal intensity for BaP determined by SALDI-MS with CHCA and MIL-100(Fe) as matrix [a].

Matrix	shot-to-shot	region-to-region	sample-to-sample
MIL-100(Fe)	2.00%	7.33%	8.59%
CHCA[b]	94.40%	46.76%	47.45%

[a] Concentration: 100 μg/mL;. Laser pulses: 500. Sample preparation: dried droplet method

[b] CHCA (10 mg) was dissolved in 1 mL H_2O/ACN (1/1, v/v) containing 0.1% TFA

35.

Table S2 Literature survey for signal reproducibility using NPs as SALDI-MS matrix

NPs	shot-to-shot[a]	analyte	ref.
14-nm Au	7.6%-8.4%	glutathione	S8
14 nm Au	5.7-8.3%	captopril	S10
Capped Au	<12%	carbohydrate	S11
Au nanoporous film	< 10%	amino acids, cyclodextrins, peptides and polyethylene glycols	S12
Carbon Nanotubes	~15%	enzyme inhibitor	S13
Graphene	14%	amino acids, anticancer drugs, nucleosides	S14
TiO_2	< 10%	catechins	S15
HgTe	< 25%	proteins, peptides	S16
CdSe quantum dot	< 10%	proteins, peptides	S17
2-10 nm Au	< 10%	peptides	S18
TiO_2	9.4%-30%	phospholipids	S19
ZnO	30%	verapamil hydrochloride, testosterone, polyethylene glycol, polystyrene, polymethylmethacrylate	S20
SBA-15	< 29%	amino acids, metabolites, saccharides, honeys.	S21
MIL-100(Fe)	2.0%-16.3%	PAHs	this work

36.

Table S3 Porosity and surface area of nanoparticles used in this work

	This work		literature	
NPs	surface area (Langmuir, $m^2 g^{-1}$)	pore size (Å)	surface area (Langmuir, $m^2 g^{-1}$)	pore size (Å)
MIL-100(Fe)	2064	5-9, 25-29	2800	5-9, 25-29
MIL-100(Cr)	1806	5-9, 25-29	3100	5-9, 25-29
MIL-100(Al)	1895	6.5, 25-29	2919	5-9, 25-29
SBA-15	707	50	780	60
14 nm Au	-	non-porous	-	non-porous

37.

Table S4 Characteristic of MOFs

MOF type	Metal center	Ligand	Pore morphology
MIL-100(Fe)	Fe^{III}	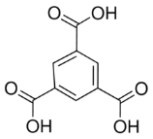	Cage
MIL-100(Cr)	Cr^{III}	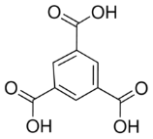	Cage
MIL-100(Al)	Al^{III}	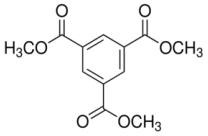	Cage
MIL-101(Cr)	Cr^{III}	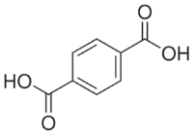	cage
DUT-4	Al^{III}	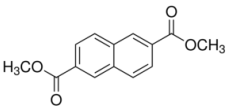	rectangular tunnels
DUT-5	Al^{III}	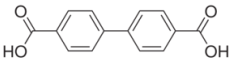	rectangular tunnels
CYCU-3	Al^{III}	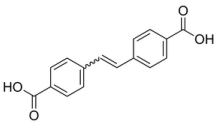	tunnel

38.

Table S5 Reproducibility of PAHs signals with different Au nanoparticles as matrix[a]

Matrix	Ant	Pyr	BaA	Chr	BaP
MIL-100(Fe)	16.33%	3.54%	5.71%	11.13%	2.00%
3.5 nm Au	-	-	30.2%	25.4%	30.8%
14 nm Au	-	-	39.4%	49.5%	22.8%
33 nm Au	-	-	13.8%	32.7%	27.9%
SBA-15	-	-	23.2%	38.5%	38.6%

[a] data (RSD of signal intensity) were obtained from five replicated experiments

- non detected

39.

Table S6 Comparison of MOFs and NPs in the preparation time, cost, background and reproducibility

	preparation time	cost	technological background	Reproducibility (batch to batch)
MOFs	30 mins-4 days	medium	coordination chemistry	high
AuNPs	3 mins-60 mins	high	chemical reduction	high
SBA-15	2 days	low	sol-gel technology	high

40.

Table S7 Effect of three sample preparation for BaP signal intensities using CHCA as matrix [a]

Sample preparation	shot-to-shot reproducibility
dried droplet	94%
two-layer	33.8%
on probe remix	33.2%

[a] data (RSD of signal intensity) were obtained with five replicated experiments

41.

Table S8 Various chromatographic methods for PAHs analysis

Literatures	Method	Analytes	LOD & analysis time
Gosettia et al. (J. Chromatogr. A, 2011, 1218, 6308)	UHPLC-APCI-MS (Qtrap)	13 PAHs	0.002-0.786 ng/mL; 22 min
Song et al. (International Journal of Mass Spectrometry, 2011, 303, 173)	LC-APCI-MS (TOF)	16 PAHs	25-30 ng/mL; 25 min
Hayen et al. (Anal. Chem., 2009, 81, 10239)	LC-APCI-MS (FTICR-MS)	6 PAHs	0.07-1.5 μg/mL; —
Chen et al. (Rapid Commun. Mass spectrum., 2007, 21, 3694)	LC-APCI-MS (QqQ)	10 PAHs	0.67-1.2 ng/kg; 26 min
Veyrand et al. (J. Chromatogr. A, 2007, 1149, 333)	GC-EI-MS	19 PAHs	0.008-0.15 μg/kg; 28 min
Aguinaga et al. (Anal. Chim. Acta, 2007, 596, 285)	GC-MS	16 PAHs	0.003-1.5 μg/L; 64 min
this work	SALDI-MS	5 PAHs	0.95-32.82 ng/mL; 1 min

42.

References

1. P. Horcajada, S. Surblé, C. Serre, D.-Y. Hong, Y.-K. Seo, J.-S. Chang, J. M. Grenéche, I. Margiolaki, G. Férey, *Chem. Commun.* **2007**, 2820.
2. G. Férey, C. Serre, C. Mellot-Draznieks, F. Millange, S. Surblé, J. Dutour, I. Margiolaki, *Angew. Chem. Int. Ed.* **2004**, *43*, 6296.
3. C. Volkringer, D. Popov,T. Loiseau, G. Férey, M. Burghammer, C. Riekel,M. Haouas, F. Taulelle, *Chem. Mater.* **2009**, *21*, 5695.
4. G. Férey, C. Mellot-Draznieks, C. Serre, F. Millange, J. Dutour, S. Surblé, I. Margiolaki, *Science* **2005**, *309*, 2040.
5. I. Senkovska, F. Hoffmann , M. Fröba, J. Getzschmann, W. Böhlmann, S. Kaskel, *Micro. Meso. Mater.* **2009**, *122*, 93.
6. S.-H. Lo, C.-H. Chien, Y.-L. Lai, C.-C. Yang, J.-J. Lee, C.-H. Lin, *J. Mater. Chem. A*, **2013**, *1*, 324.
7. M.-F. Huang, C.-C. Huang, H.-T. Chang, *Electrophoresis* 2003, **24**, *2896*.
8. C.-K. Chiang, Y.-W. Lin, W.-T. Chen, H.-T. Chang, *Nanomedicine NBM* **2010**, *6*, 530.
9. D. Zhao, Q. Huo, J. Feng, B. F. Chmelka, G. D. Stucky, *J. Am. Chem. Soc.* **1998**, *120*, 6024.
10. W.-T. Chen, C.-K. Chiang, Y.-W. Lin, H.-T. Chang, *J. Am. Soc. Mass. Spectrom.* **2010**, *21*, 864.
11. C.-L. Su, W.-L. Tseng, *Anal. Chem.* **2007**, *79*, 1626.
12. R. Liu, J.-F. Liu, X.-Xia Zhou, G.-Bin Jiang, *Anal. Chem.* **2011**, *83*, 3668.
13. S. Xu, Y. Li, H. Zou, J. Qiu, Z. Guo, B. Guo, *Anal. Chem.* **2003**, *75*, 6191.
14. X. Dong, J. Cheng, J. Li, Y. Wang, *Anal. Chem.* **2010**, *82*, 6208
15. K.-H. Lee, C.-K. Chiang, Z.-H. Lin, H.-T. Chang, *Rapid Commun. Mass Spectrom.* **2007**, *21*, 2023.
16. C.-K. Chiang, Z. Yang, Y.-W. Lin, W.-T. Chen, H.-J. Lin, H.-T. Chang, *Anal. Chem.* **2010**, *82*, 4543.
17. K. Shrivas, S. K. Kailasa, H.-F. Wu, *Proteomics* **2009**, *9*, 2656.
18. J. A. McLean, K. A. Stumpo, D. H. Russell, *J. Am. Chem. Soc.* **2005**, *157*, 5304.
19. P. Lorkiewicz, M. C. Yappert, *Anal. Chem.* **2009**, *81*, 6596.
20. T. Watanabe, H. Kawasaki, T. Yonezawa, R. Arakawa, *J. Mass Spectrom.* **2008**, *43*, 1063.
21. X. Li, X. Wu, J. M. Kim, S. S. Kim, M. Jin, D. Lia, *J Am Soc Mass Spectrom.* **2009**, *20*, 2167.